Available online at www.sciencedirect.com
ScienceDirect
Applied Geochemistry 22 (2007) 2486–2508
Applied Geochemistry
www.elsevier.com/locate/apgeochem

Formation of sequences of cemented layers and hardpans within sulfide-bearing mine tailings (mine district Freiberg, Germany)

Torsten Graupner [a,*], Andrea Kassahun [b], Dieter Rammlmair [a], Jeannet A. Meima [a], Dagmar Kock [a], Markus Furche [a], Adrian Fiege [a], Axel Schippers [a], Frank Melcher [a]

[a] *Federal Institute for Geosciences and Natural Resources (BGR), Stilleweg 2, 30655 Hannover, Germany*
[b] *Groundwater Research Institute (GFI), Meraner Strasse 10, 01217 Dresden, Germany*

Received 9 February 2007; accepted 11 July 2007
Editorial handling by B. Kimball
Available online 21 July 2007

Abstract

The roles of mineral dissolution, precipitation, transformation and mass transport processes related to formation of characteristic cemented layer–hardpan sequences were studied in low sulfide and low carbonate Freiberg polymetallic mine tailings. Using high resolution profiling, combined geochemical, geomicrobiological and geophysical methods allowed description of the process of weathering of reactive mineral phases and the position of the oxidation front in detail, as well as revealing the mechanisms of cementation of tailings predominantly by the formation of gels/poorly crystalline phases. Autochthonous and allochthonous gels reduced the porosity of cemented layers to values $\leqslant 1\%$, whereas secondary crystalline phases were less efficient in filling the pore space. Electron microprobe analysis of cemented tailings showed that common jarosite-group minerals contained up to about 8 wt.% PbO and 0.2–1.9 wt.% As_2O_5. Iron–As–Si gels reached contents of up to ~44 wt.% As_2O_5 in gel-rich cemented layers. Zinc was below the detection limit in the studied secondary phases. Sequential extraction of cemented and related oxidized brown silt layers confirmed that the bulk of As was bound to amorphous/poorly crystalline hydrous oxides of Fe, whereas Pb was often bound to jarosite. Zinc was found preferentially in the water-soluble and the exchangeable fractions. In the grey silt and the sand directly underlying the oxidized layers, As, Pb and Zn occurred as sulfide minerals. The main effects of the cemented layer–hardpan sequences at the studied site are (1) a temporary natural attenuation of the toxic compounds, (2) a restriction of the downward movement of the oxidation front, and (3) a reduction of the extent of the erosion of the surface of the tailings impoundment by wind and water. The potential of a heap to form cemented layers and hardpans is greatly increased by a heterogeneous distribution of grain sizes and reactive materials in the topmost zone, as well as by the occurrence of sulfide-rich tailings on top of layers with low permeability.

* Corresponding author.
E-mail address: torsten84@gmx.de (T. Graupner).

0883-2927/$ - see front matter © 2007 Elsevier Ltd. All rights reserved.
doi:10.1016/j.apgeochem.2007.07.002

1. Introduction

The study of natural attenuation (NA) processes on Acid Mine Drainage (AMD) formation in mine waste deposits is of great importance, because NA may counteract serious pollution threats to the water systems. Mobilisation of As, Zn and Pb from metallic mine tailings is known to be induced by oxidative weathering of metal sulfides. For example, oxidation of arsenopyrite (FeAsS) and Fe^{2+}-bearing sphalerite ((Zn,Fe)S) results in AMD containing H_2SO_4, Fe(III) as amorphous ferric oxyhydroxide precipitates, Fe(II) as soluble Fe species, As(III) as arsenite (AsO_3^{3-}), As(V) as arsenate (AsO_4^{3-}), and Zn(II). Microorganisms are known to catalyze sulfide oxidation (e.g. *Acidithiobacillus ferrooxidans*, *Thiomonas* sp.; e.g. Tuovinen et al., 1994; Blowes et al., 1998; Bruneel et al., 2003; Schippers, 2004; Morin and Calas, 2006). Several contaminant attenuation processes in mine waste deposits must be considered, like precipitation, sorption, and ion substitution. For example, arsenate may precipitate as scorodite, $FeAsO_4 \cdot 2H_2O$ (Ehrlich, 2002) or more commonly as ferric arsenate (Paktunc et al., 2004), sorb to amorphous ferric oxyhydroxide phases and clay minerals (e.g. Korte and Fernando, 1991), or substitute for sulfate in jarosite, $KFe_3(SO_4)_2(OH)_6$ (e.g. Paktunc and Dutrizac, 2003; Waychunas et al., 1995). Because hardpans and cemented layers may consist of reactive secondary minerals, they are expected to play a crucial role in contaminant attenuation.

Cemented, indurated layers in sulfide-bearing mine tailings (so-called hardpans) have been studied for their physical, chemical and mineralogical properties (Blowes and Jambor, 1990; Tassé et al., 1997; Coggans et al., 1999; Johnson et al., 2000; McGregor and Blowes, 2002; Courtin-Nomade et al., 2003; Giere et al., 2003; Gilbert et al., 2003; Moncur et al., 2005; Gunsinger et al., 2006). Field studies have reported on hardpans in e.g. Canadian tailings impoundments (McGregor and Blowes, 2002; Moncur et al., 2005; Gunsinger et al., 2006). The thickness of the hardpans varied from a few cm up to ~4 m. They consisted of ferrihydrite ($Fe_2O_3 \cdot 0.5\ H_2O$), gypsum ($CaSO_4 \cdot 2H_2O$), jarosite, lepidocrocite (γ-FeOOH), melanterite ($FeSO_4 \cdot 7H_2O$), and rozenite ($FeSO_4 \cdot 4H_2O$). The highest concentrations of originally dissolved metals were observed directly above and within a hardpan layer, thus the hardpans may have restricted the movement of dissolved metals through the tailings and may have acted as a zone of metal accumulation. In addition, the permeability of the hardpans was lower than that of uncemented tailings. Column experiments verified that hardpans that are situated between reactive tailings and cover material, improved leachate water quality and reduced the rate of sulfide oxidation (Gilbert et al., 2003).

The terms hardpan and cemented layer are widely used, but these terms are not exactly defined in the literature. In the authors' understanding, hardpans are zones at the capillary fringes where agglutination of particles is basically due to processes driven by capillary transport within an O_2 dominated environment. Supersaturation results in the precipitation of secondary phases and gels, which may coat particles, agglutinate them, and reduce the porosity. Cemented layers on the other hand, can be observed at the transition between oxidized and reduced zones, which often occurs at the transition between saturated and unsaturated zones. At these transitions, variations in master geochemical variables, such as Eh and pH, occur.

Despite that hardpan layers probably play a pivotal role in the NA of unwanted metals that may originate from sulfide-bearing mine tailings, their formation processes have not been thoroughly studied. A combination of processes such as dissolution of primary mineral phases, transport processes, and precipitation of secondary phases seems to be responsible for hardpan/cemented layer formation in mine tailings. The formation of amorphous phases (gels) and/or poorly crystalline phases plays a key role in this process. Gel formation has been documented for a wide range of geochemical conditions; they occur in alkaline (pH 9–14; Wan et al., 2004; Rammlmair et al., 2005) and also in neutral to acidic, sulfate-rich environments (pH < 1–6; e.g. in AMD; Rousel et al., 1999). However, the mechanisms of formation of gel-rich layers in tailings, their distribution characteristics and stability, as well as possible genetic relationships between gel-rich layers and sulfate-rich hardpans are controversially discussed or lacking in the literature.

A multi-disciplinary approach based on geochemical, mineralogical, geophysical and geomicrobiological methods was applied to study (i) the mechanism of formation of gel-rich and gel-poor cemented layers and hardpans in an AMD environment, and (ii) the NA capacity of the cemented layers and hardpans for As, Pb and Zn. The low-sulfide and low-carbonate tailings deposited at the studied site represent a major type of tailings impoundment of great international importance (e.g. Diaby et al., 2007).

2. Material and methods

2.1. Site description

The Muenzbachtal tailings impoundment (polymetallic sulfide mine district Freiberg, Saxony, Germany) is ~320 m wide, has a maximum height of ~30 m and an almost flat plateau which covers an area of ~60,000 m^2 (Fig. 1a). It was used to deposit sulfide-bearing tailings from 1955 to 1968. The volume of the deposited material was estimated at ~835,000 m^3 (1.3 Mt; ACD report, 1993). It almost exclusively derived from the processing plant of the "Grube Beihilfe" mine in Halsbruecke, which produced Pb–Zn concentrate using ore from the hydrothermal "Halsbruecker"-, "Ludwig"-, and "Drei Prinzen-Spat" veins. The metal content of the original heap material was determined at ~0.1 wt.% Pb, ~0.2 wt.% Zn, ~1.4 wt.% S, 0.02 wt.% Cu and ~0.1 wt.% As (ACD report, 1993). After termination of deposition, the tailings impoundment was partly covered with coarse sand and topsoil (thickness of cover: ⩽0.2 m).

2.2. Profiling methods

The depth of the oxidation zone was investigated in a SE-NW profile using a drilling stock (Fig. 1a). For each location, two samples of unaltered material were collected from a depth of ~1.6–1.8 m. These samples were analysed for particle-size distribution using an automatic particle-size analyser (<63 μm fraction; Micrometrics SediGraph 5100) which is based on X-ray scattering.

2.3. Geophysical methods

The apparent resistivity was measured along three profiles parallel to and two profiles across the Muenzbach stream in a Wenner configuration

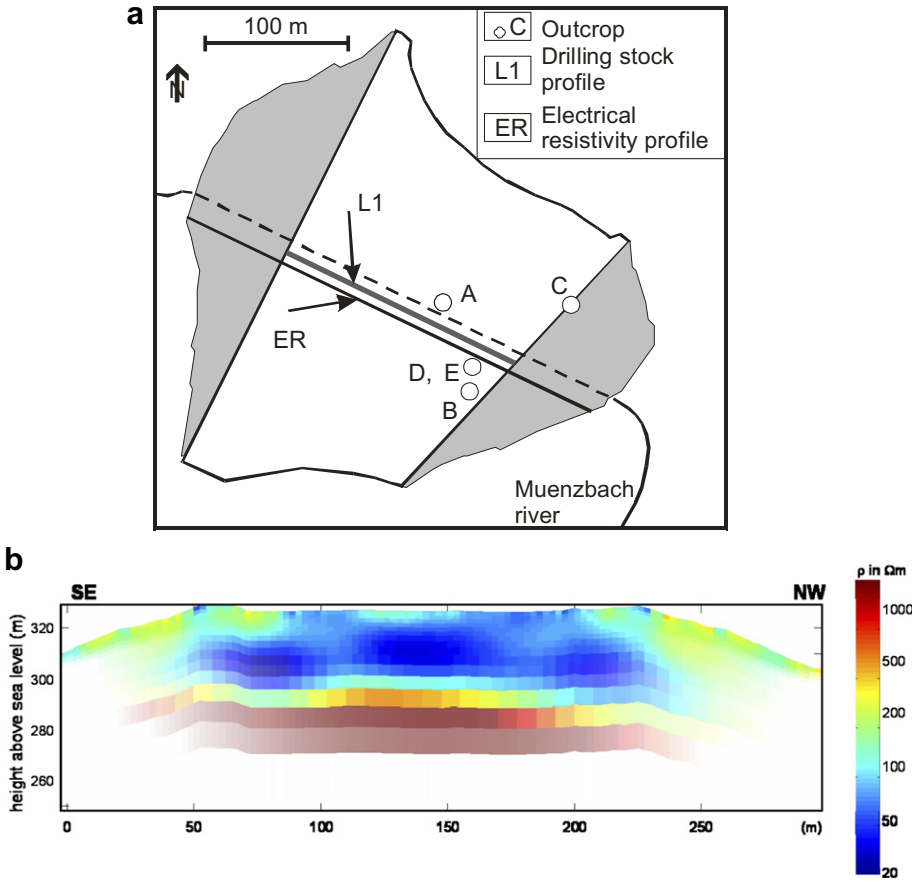

Fig. 1. (a) Schematic map of the Muenzbachtal tailings impoundment showing the locations of the profiles discussed here. (b) 2D cross section of electrical resistivity parallel to the Muenzbach stream from SE to NW.

ranging over the whole dump body. These data were used to compute 2D-models of resistivity distribution using a finite difference (FD) inversion technique. Since resistivity is a function of porosity, water conductivity, and water content of sediments, the resistivity models give a qualitative impression of grain size distribution and water content of the tailings assuming a constant conductivity of water (Archie, 1942).

The measurement of spectral induced polarisation (SIP) records the amplitude of resistivity and, additionally, the time delay between voltage signal and the injected current for different frequencies. In the frequency domain, this time delay corresponds to a negative phase angle between current and voltage. Phase shifts are mainly caused by polarizable materials (e.g. sulfides; Pelton et al., 1976).

2.4. Geochemical and mineralogical methods

Sequential extractions were used for determination of pollutant content and speciation within the dump pore waters and mineral phases (cf. Dold, 2003; Gault et al., 2005). Selective dissolution of mineral phases was achieved applying a sequential extraction method modified from that of Zeien (1995). Table 1 contains the extraction sequence including the expected phases that would dissolve in each extraction step. Sequential extractions were performed at 2.5–5.0 g of sediment samples. Samples were placed in 100 mL borosilicate glass centrifuge tubes, reacted with 50 mL of solvent solution and centrifuged after each extraction step (steps I–VIII). For aqua regia dissolution (step IX), samples were transferred to teflon vessels and reacted in a microwave extraction unit. Multi-element chemical analysis was performed on supernatant liquids using ICP-OES (Spectro Ciros^{CCD}). Merck multi element standards and an As standard were used for calibration. Detection limits were 0.01 mg/L for As, Pb and Zn, 0.02 mg/L for Fe and Mg analysis, 0.05 mg/L for Al, Ca and Na, 0.1 mg/L for K and Si, and 0.3 mg/L for S. Inorganic C analysis by conversion to CO_2 and subsequent IR detection (Shimadzu TOC-$V_{CPH/CPN}$) had a detection limit of 0.5 mg/L.

Frequency distributions were estimated for mineral and amorphous phases as well as for open or partially filled pore spaces within cemented layers, hardpans and unconsolidated sediments. A 4-step procedure was applied: (i) Mapping of element distribution within a profile of adjacent areas of $\sim 3 \times \sim 3$ mm in polished thin sections that were not coated with C. Mapping was carried out with the EDAX module (C Kα, Si Kα, Al Kα, Ca Kα, S Kα, Ba Lα, Fe Kα, As Kα) of a Quanta 600 FEG system (FEI Company) using a maps resolution of 512×512 (dwell time: 400 μs; 64 frames). (ii) Based on microscopic studies, rectangular regions of interest (ROI) were defined for (a) cemented and (b) loose parts of the mapped areas. These ROIs were representative of the studied zones. (iii) Each mineral phase as well as the open or partially filled pore space was described by a special element signature (Table 2). For some phases, two or more elements were combined, or the signal of other phases was subtracted to separate them clearly (e.g. combination of Ca and S for gypsum). (iv) For processing of false colored images the Analysis© system was used. The averaging filter was applied to erase artefacts. Combined images of

Table 1
Extraction protocol (modified from Zeien, 1995)

Extraction step	Solvent	Extracted pollutant fractions
I	Aqua dest.; 2 h	Pore water, sulfate minerals
II	1 M $SrCl_2$; 30 min; twice	Cation exchange complex
III	1 M NH_4OAc; pH 6; 12 h; repeat until $TIC_{extract} = 0$	Carbonates
IV	1 M NH_4OAc + 0.1 M NH_2OH; pH 6; 30 min	Easily reducible phases (e.g. Mn oxides)
V	0.025 M NH_4–EDTA; pH 4.7; 90 min	Organic matter, hydrated Si gels
VI	0.2 M NH_4-oxalate; pH 3.3; 4 h (in darkness)	Poorly crystalline Fe oxyhydroxides (e.g. ferrihydrite) and jarosite-group minerals, dehydrated Si gels
VII	0.2 NH_4-oxalate + 0.1 M ascorbic acid; 30 min; boiling (water bath); pH 3	Crystalline Fe oxides (e.g. goethite, hematite) and jarosite, Al oxyhydroxides, aluminosilicates (minor)
VIII	8.8 M H_2O_2; pH 2; at room temperature until end of degassing (7–14 d)	Sulfides (e.g. ZnS, PbS, FeS_2), aluminosilicates
IX	Aqua regia; 180 °C; 20 bar; 15 min	Sulfides (e.g. PbS, ZnS) enclosed in silicates, aluminosilicates

Table 2
Processing of data for estimation of frequency distributions of mineral phases and pore spaces

Phase	Filters	Operations	Images
Pore space	N × N	–	C Kα
Barite ($BaSO_4$)	Ave	–	Ba L
Sulfide–pyrite (FeS_2)	Sigma, Ave	Fe Kα × S Kα	S Kα, Fe Kα
Gypsum ($CaSO_4 \cdot 2H_2O$)	Ave	Ca Kα × S Kα	Ca Kα, S Kα
Fluorite (CaF_2)	DCE, Ave	Gypsum (inverted) × Ca Kα	Ca Kα, gypsum
Quartz (SiO_2)	DCE, Ave	Invert Fe Kα, K Kα, …; multiply each with Si Kα	Si Kα, Fe Kα, K Kα, Ca Kα, Al Kα
Silicates (excl. quartz)	N × N, Ave	Quartz (inverted) × Si Kα	Si Kα, quartz
Fe phases (excl. sulfides)	Ave	Sulfide (inverted) × Fe Kα = X; Si Kα (inverted) × X	Si Kα, Fe Kα, sulfide (pyrite)
As-bearing phases (MIA)	N × N	Coordinate the images without correlation	As Kα

Filters: Ave – averaging filter; DCE – differential contrast enhancement; N × N – definition of parameters for averaging filter with optional square matrix; Sigma – filtering of the shot noise. MIA – multiple image alignment.

two or more elements were edited using filters to optimize the fitting threshold. Table 2 specifies the elements used for each studied phase, as well as the filters and operations applied.

For XRD analysis, a Philips PW 3710 series automated powder diffractometer was employed which uses Cu radiation (Kα line with a mean wavelength of 1.542 Å) operated at 40 kV and 30 mA, and glancing angles 2θ between 2° and 65°. A secondary graphite crystal monochromator was used. For evaluation of the data the software package Galaxy linked with a PDF2 data base was employed.

Electron microprobe (EM; CAMECA SX-100 microprobe) analysis was applied to study amorphous and poorly crystalline Fe(III) phases, jarosite-group minerals and gypsum from cemented layers as well as from unconsolidated oxidized sediment for their compositions and NA capability concerning the contaminants. Operating conditions were a 15 kV accelerating voltage and a 20 nA beam current. Mineral standards were used and data were obtained using a TAP crystal for Si Kα, Al Kα, Mg Kα, Na Kα and As Lα analysis, a PET crystal for K Kα, Ca Kα, Pb Mα and S Kα, and a LiF crystal for Fe Kα and Zn Kα. Detection limits under the applied measurement conditions were 0.15 wt.% for As and Fe, 0.10 wt.% for Pb and Zn, and 0.05 wt.% for S, Si, Ca, Na, Al, K and Mg.

2.5. Microbiological methods

The number of metal sulfide oxidizing microorganisms was determined by the "most probable number" technique (MPN) as previously described by Schippers and Bosecker (2005). Two different media were used for enrichment of acidophilic Fe(II) oxidizers of the type *A. ferrooxidans* (Leathen et al., 1951) and S-oxidizers of the type *Acidithiobacillus thiooxidans* (Starkey, 1925). The concept of the MPN is described elsewhere (Cochran, 1950). Two grams of tailings material was suspended in 20 mL of medium for Fe(II) oxidizers without substrate (i.e. without Fe(II) sulfate). The suspension was incubated for 2 h on a rotary shaker at 130 rpm to detach cells from the substratum. The suspension was diluted in 10-fold steps to 10^{-8} and used to inoculate the MPN tubes. Cultures were incubated on a rotary shaker (130 rpm) in the dark at 30 °C for 3 weeks. The tubes were counted as positive if the pH had dropped below a value of 2 (S oxidizers) or if Fe(III) was formed (Fe(II) oxidizers).

3. Results and discussion

3.1. Internal structure of the tailings impoundment

The 2D cross section of electrical resistivity (Fig. 1b) shows four zones for the tailings impoundment: (i) the basement as indicated by resistivities of >1000 Ωm, (ii) the slimes area of the tailings impoundment as characterized by resistivities of <50 Ωm, (iii) the sandy tailings near the slopes with intermediate resistivities, and (iv) the sandy slopes with intermediate resistivity values as well. The different resistivities measured for the central part (slimes area) and the edges and slopes of the dam are explained by a particle-size induced difference in water content and due probably to elevated ion contents of the solution in the capillary fringe (Furche et al., 2007). The grain size distribution (Fig. 2b) indicates that the central part mainly consists of silt and fine sand, and that

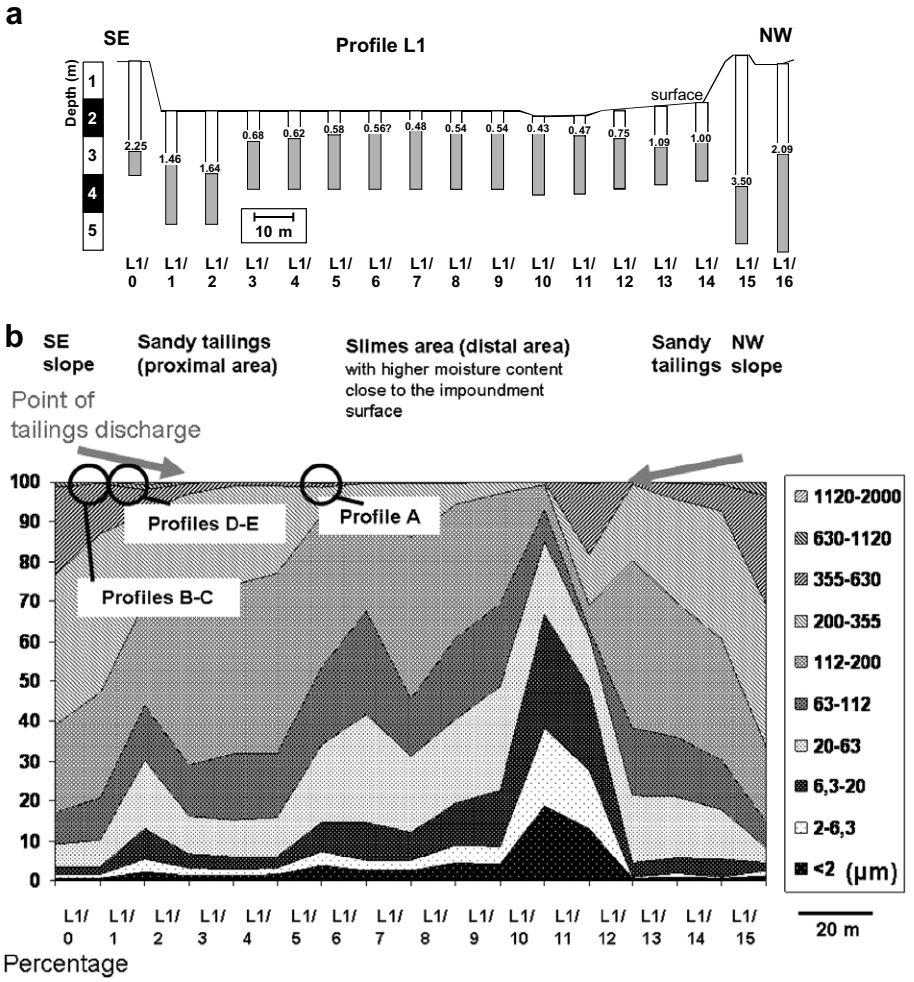

Fig. 2. (a) and (b) SE-NW drilling stock profile across the Muenzbachtal tailings impoundment. (a) The depth of the transition between the unaltered material (grey part of column) and the oxidized zone (unfilled upper part of column) is added for each location. (b) Grain size distribution of unaltered material at each location (depth for samples L1/1–14: ~1.6–1.8 m); average of duplicate measurements is plotted.

the edges and slopes of the dam mainly consist of fine to medium graded sand.

Numerous delta systems overlie each other due to the spill displacement along the rims of the dam. Mineral segregation resulting from this process favoured the development of heavy mineral rich (e.g. sulfides) layers due to sedimentary enrichment processes. The loamy parts of the tailings impoundment are characterized by graded bedding on cm-scale. The sandy tailings locally show a strong variability caused by complex depositional patterns. This variability is characterized by (i) interlayered packages with different alteration behaviour, (ii) the presence of (locally multiple) thin silt layers, and (iii) the occurrence of thin sulfide-enriched layers or lenses, which may, in the case of extremely sulfide-enriched layers, result from malfunctions during processing of the ore.

The slimes area and sandy tailings show differences concerning the depth of the oxidation front and the development and extent of the cemented layers and hardpans formed. The depth of the oxidation front was <0.4 to ~0.5 m for the silty slimes. It increased to values between 1.6 and >3.0 m for the sandy tailings at the slopes of the dam (Fig. 2a). The transition between oxidized and unaltered zones is commonly marked by one or more thin greyish (weakly altered) silt layers. The specific surface areas of the material show an increase from values of ~2 to ~4 m^2/g in the unaltered material to values up to ~9 m^2/g in the oxidized zone (Jung, 2003).

3.2. Distribution of cemented layers and hardpans

At the edges of the slimes area, cemented layers were ⩽1 cm thick and their occurrence was essentially limited to a narrow zone between the unaltered and oxidized zones (e.g. profile A). Fig. 3 gives a depth profile for outcrop A (for position see Figs. 1a and 2b). The topmost part of profile A consists of ~0.10 m top soil as covering material, followed by a ~0.50 m thick sequence of oxidized sands with small lenses of weathered silt. Multiple, 2–5 mm thin, but more or less continuously developed cemented layers occur in the depth range between 0.57 and 0.65 m; they were always directly underlain by altered silt layers. At greater depth, this sequence was followed by several thin and essentially unaltered silt layers, with color changes from brown to grey in associated fine sand layers.

In the sandy tailings, multiple cemented layers and hardpans were observed. Fig. 4 gives examples of depth profiles which were situated in the sandy tailings at the edge of the tailings impoundment. Cemented layers occurred in the lower parts of the oxidized zone only. Hardpans were mostly formed in the upper part of the oxidized zone. Cemented layers and hardpans were present (i) as horizontal layers or (ii) as lens-shaped bodies (Fig. 4). Hardpan layers often were interbedded with <0.1 cm layers of loose material, forming packages ranging in thickness from <1.0 cm to ⩾20 cm. Lens-shaped hardpans may reach a thickness of ⩾30 cm as shown in Fig. 4 for profile B. Silt layers, or systems of fine

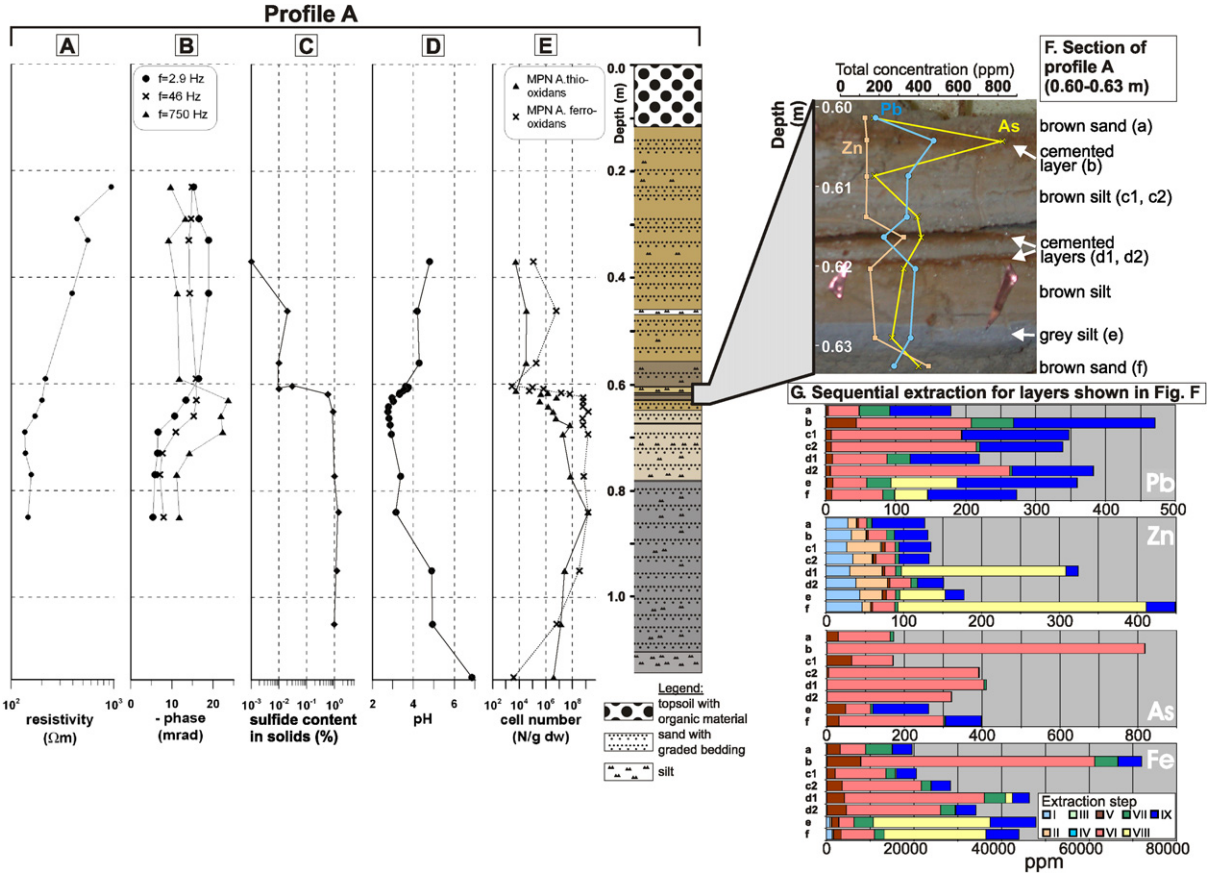

Fig. 3. (A) to (G) Geophysical, geochemical and geomicrobiological profiles through the oxidized zone in the marginal part of the slimes area (profile A). (A) and (B) Results of SIP measurements at different depth (resistivity; phase values for three frequencies). (C) Sulfide content in solids. (D) pH values. (E) MPN values for acidophilic Fe(II) oxidizers (*Acidithiobacillus ferrooxidans*) and sulfur oxidizers (*Acidithiobacillus thiooxidans*). (F) Section of profile A showing the zone where the oxidation front is located. (G) Release of Pb, Zn, As and Fe during sequential extraction for layers a to f as shown in the detailed profile (F). Extraction steps: I – water soluble fraction; II – exchangeable fraction; III – carbonates; IV – Mn oxides; V– organic matter, hydrated Si gels; VI – poorly crystalline Fe oxyhydroxides, jarosite-group minerals; VII – crystalline Fe oxyhydroxides, jarosite-group minerals; VIII – sulfides, alumosilicates; IX – alumosilicates with sulfide inclusions; for more details see Table 1 and text.

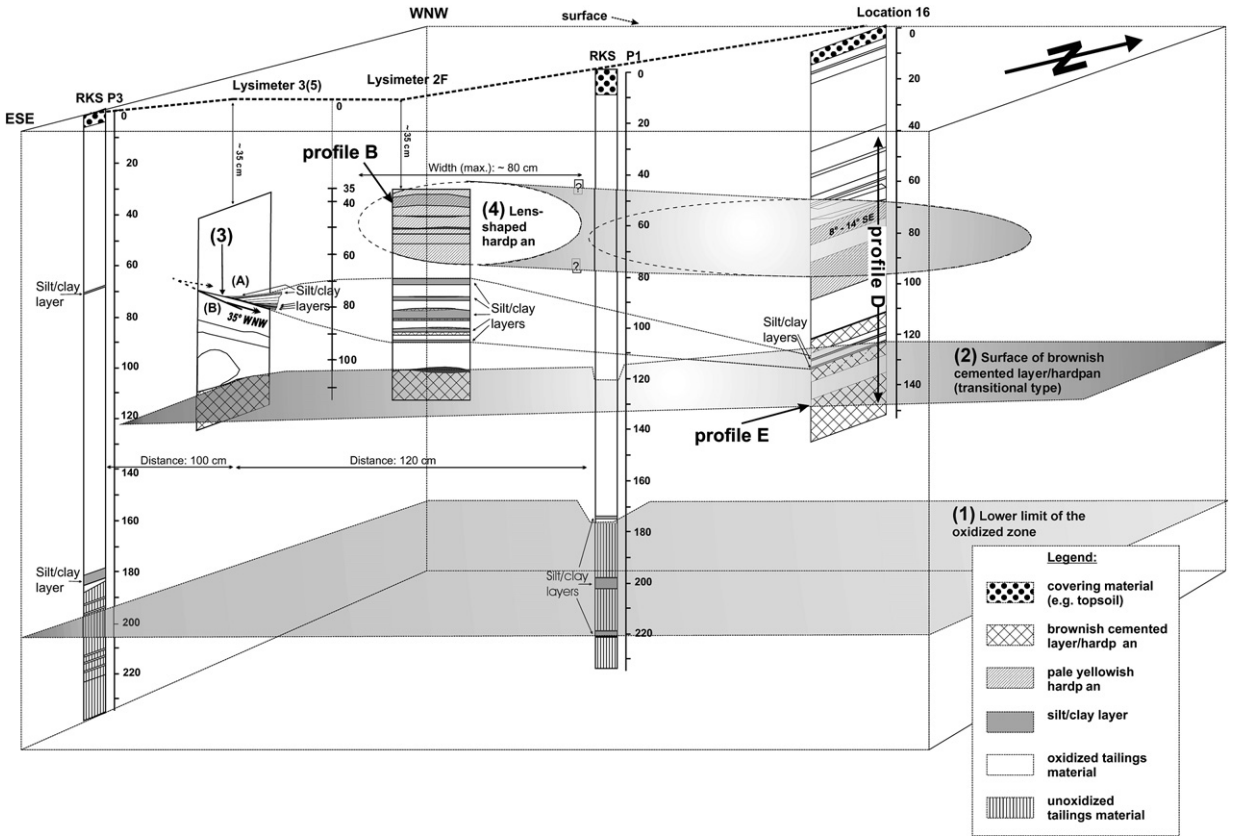

Fig. 4. Internal structure of the SE margin of the sandy tailings (Muenzbachtal tailings impoundment). Highlighted depositional and alteration structures are (from bottom to top of profile): (1) The lower limit of the oxidized zone; (2) The surface of a brownish cemented layer/hardpan as found in all outcrops; (3) The WNW dipping margin of the SE slope of the impoundment separating (A) the sandy tailings and (B) the slope; (4) A lens-shaped pale-yellowish hardpan overlying a system of altered silt/clay layers with brownish cemented layers. Depth is given in centimeters if not otherwise stated.

sand/silt layers, were usually present below cemented layer–hardpan sequences.

3.3. Mineralogical composition of the heaped material

3.3.1. Primary phases

Primary phases at the tailings impoundment include: fragments of the Freiberg gneiss (for modal mineralogy of the rock see e.g. Tichomirowa, 2001), hydrothermal vein quartz, barite, fluorite, pyrite, arsenopyrite, sphalerite and galena, minerals probably formed in the oxidation zone of the hydrothermal ore veins (e.g. anglesite, $PbSO_4$; cuprite, Cu_2O) and also subordinate technical products.

Unaltered silt layers were enriched in sulfides and strongly enriched in micas compared to unaltered sandy tailings. Heavy mineral-rich layers deposited directly on top of the silt were enriched in barite, sulfides and accessory minerals (e.g. zircon), especially in the outer (less fine-grained) zones of the slimes area. Unaltered sandy tailings were mainly composed of quartz, feldspar and fluorite, and contained only low concentrations of sulfides.

In the oxidized zone, arsenopyrite and sphalerite were completely replaced in all tailings materials, whereas pyrite and galena were often partly replaced only in heavy mineral-rich layers (arsenopyrite is more reactive than pyrite; e.g. Blowes et al., 2005). The only sulfide occasionally found in sandy materials is galena, commonly with rims of anglesite. Oxidation of galena is probably retarded due to the covering of their surfaces with oxidation products (e.g. Haubrich et al., 2000; Tichomirowa et al., 2002). Carbonates were scarce in the unaltered material and absent in the oxidized tailings materials. Chemical decomposition of mica and plagioclase was widespread and provided a source of Si, Al, K and Ca especially in the silt layers.

3.3.2. Secondary phases

Secondary phases most frequently formed in the oxidized zone of the tailings impoundment were gypsum, Fe(III) oxyhydroxides, and Fe(III) oxysulfates (i.e. jarosite). Additionally, Si-, Si–Fe-, or Fe–As-rich gels, alunite, native S, a ferric arsenate precipitate which shows a composition similar to scorodite, and clay minerals occurred. In the <2 μm fraction of a sample from profile A (Fig. 3), the following clay minerals were identified by XRD: kaolinite, an irregular illite-dominated illite(0.7)-smectite(0.3) mixed-layer clay, and possibly chlorite.

Thin layers of autochthonous gels encrusted reactive sulfides shortly after the first contact with rain water. These gels generally consisted of Fe(III)-rich, relatively S-poor and commonly Si-bearing phases. They outlined the contours (skins) of the replaced sulfide fragments (Rammlmair, 1996) or highlighted micro-cracks starting from the surface of the altered mineral grain (formation of "honeycomb-like" textures at originally sulfide-rich locations; Fig. 5b). The degree of fill of the space inside the "honeycombs" varies considerably (see below). Multiple thin layers of allochthonous gels agglutinated mineral fragments and dust in pore spaces or covered fluid channels with cemented material (Fig. 5a).

3.3.2.1. Gel-rich environments. In extremely reactive mineral-rich mine tailings layers, the pores of the material were almost completely filled with allochthonous gel (poorly crystalline) phases as a result of oxidative dissolution of reactive sulfide minerals (profile C; Fig. 5a). Water circulation, and also mobilisation and transport of ions were essentially restricted to a small number of remaining fluid channels (Fig. 5a).

Cemented tailings in such environments showed multiple layers of poorly crystalline Fe(III)–As–S

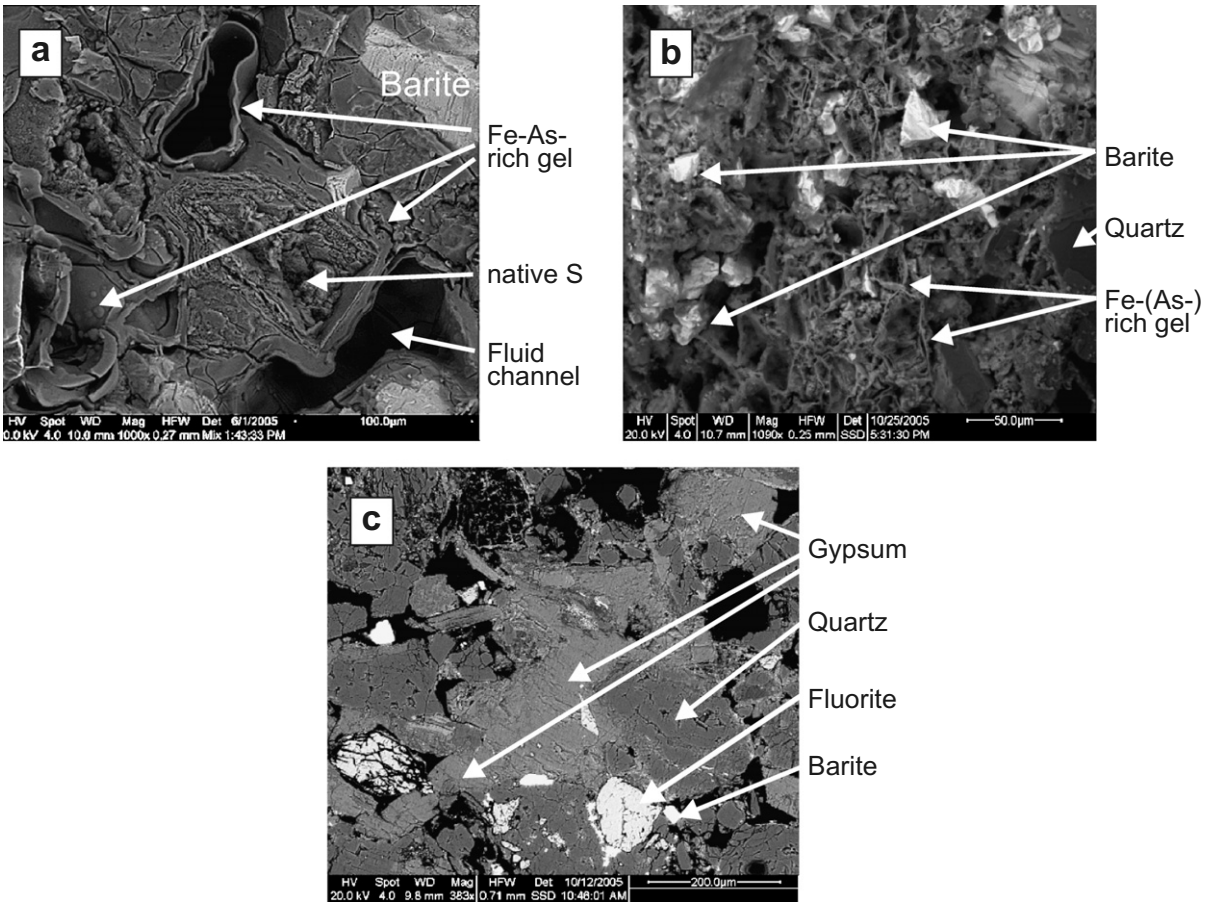

Fig. 5. (a)–(c): BSE images of weathered tailings material from the Muenzbachtal tailings impoundment: (a) Fe–As–Si gel-rich cemented layer. Note the occurrence of a high percentage of allochthonous gel and a limited number of coated fluid channels (profile C; ESEM-mixed image). (b) "Honeycomb-like" texture of autochthonous Fe–As–Si gels in a moderately gel-bearing cemented heavy mineral-rich layer overlying an altered silt layer (profile A). (c) Sediment cemented with gypsum (profile C).

Table 3
Results of electron microprobe analyses of jarosite-group minerals and poorly crystalline phases from cemented mine tailings materials (Muenzbachtal tailings impoundment, profiles C and D)

	Jarosite								Embedding material		Poorly crystalline phases (Fe–As–Si gels)						Arsenopyrite
	In sulfate-rich hardpans[a]				In packages with inter-laminated mica and heavy mineral-rich layers and lenses[b]						In sulfate-rich hardpans[a]		In a gel-rich cemented layer[c]				
	J19	J20	J22	J24	J34	J36	J39	J40			X13	X16	X1	X15	X17	X18	
Al_2O_3, wt.%	b.d.	b.d.	0.06	b.d.	b.d.	b.d.	0.05	b.d.	b.d.	Al_2O_3, wt.%	0.36	0.58	b.d.	0.13	0.06	b.d.	
Fe_2O_3	42.45	45.90[d]	42.36	42.18	39.26	38.34	39.88	37.51	b.d.	Fe_2O_3	29.34	48.17	39.70	35.84	39.71	40.34	
MgO	0.10	b.d.	0.10	b.d.	b.d.	b.d.	b.d.	b.d.	b.d.	MgO	b.d.	b.d.	b.d.	b.d.	b.d.	b.d.	
CaO	0.11	0.07	0.08	0.09	0.24	0.11	0.23	0.14	b.d.	CaO	0.12	0.24	0.16	0.14	0.14	0.28	
Na_2O	1.69	1.53	1.87	2.21	0.19	0.15	0.15	0.21	b.d.	Na_2O	0.16	0.23	b.d.	0.06	b.d.	b.d.	
K_2O	3.81	4.00	3.72	3.90	4.24	4.13	4.81	4.46	b.d.	K_2O	0.26	0.51	b.d.	b.d.	b.d.	b.d.	
PbO	1.74	0.86	0.69	0.52	8.09	7.53	7.91	6.64	b.d.	PbO	b.d.	0.87	1.66	1.43	1.69	1.97	
SO_3	28.18	30.55	28.50	28.00	27.41	26.39	27.48	27.19	0.23	ZnO	b.d.	b.d.	b.d.	b.d.	b.d.	b.d.	
As_2O_5	0.18	0.16	0.15	0.25	1.47	1.08	1.91	1.25	b.d.	SO_3	3.94	8.57	5.79	5.97	6.72	7.42	
H_2O	9.82	10.81	10.12	9.69	10.92	10.10	10.99	11.23		As_2O_5	2.40	3.73	40.33	41.72	42.11	44.23	
										SiO_2	4.29	10.67[e]	2.72	4.62	0.34	0.50	
Total	88.08	93.89	87.70	86.92	91.85	87.88	93.45	88.68		Total	40.91	73.58	90.43	89.94	90.84	94.85	
Fe^{3+}	3.00	3.00	2.97	3.00	2.77	2.83	2.78	2.68		Fe	34.3	34.3	34.3	34.3	34.3	34.3	34.3
Mg	0.00	0.00	0.00	0.00	0.00	0.00	0.00	0.00		As[f]	2.6	2.5	32.5	37.2	33.9	35.1	46.0
Ca	0.00	0.00	0.00	0.00	0.00	0.00	0.00	0.00		As loss[g] (%)	*94*	*95*	*29*	19	26	*24*	
Na	0.31	0.26	0.34	0.40	0.03	0.03	0.03	0.04		S[f]	0.9	3.4	1.9	1.7	2.2	2.4	19.7
K	0.46	0.44	0.44	0.47	0.51	0.52	0.56	0.54		S loss[g] (%)	*95*	*83*	*90*	*91*	*89*	*88*	
Pb^{2+}	0.04	0.02	0.02	0.01	0.20	0.20	0.20	0.17									
H_3O^+	0.15	0.26	0.18	0.11	0.06	0.05	0.01	0.08									
$SO_4 + AsO_4$	2	2	2	2	2	2	2	2									

b.d. – below LOD.
[a] Sample FB(05)16-KP11.
[b] Sample FB(05)16W.
[c] Sample FB(05)14-KP2.
[d] Value corrected for intergrown Fe oxyhydroxide.
[e] Si value probably contaminated from underlying quartz grain.
[f] As and S concentrations normalized to stoichiometric FeAsS mineral composition.
[g] Estimated maximum loss of As and S during oxidative weathering of sulfides assuming ideal FeAsS composition of original sulfides (not arsenical pyrite).

phases and aggregates of native S inside the ''honeycombs''; jarosite crystals were absent here. Up to several wt.% of Si, which was distributed heterogeneously, occurred in the outermost autochthonous gel rims (skins) only (analyses X1, X15 and X18 in Table 3), whereas the internal layers with low crystallinity were generally low in Si (e.g. analysis X17 in Table 3). This observation points to a development of Si networks with polyvalent cations in gel layers accessible for Si-bearing pore solutions (cf. formation of stable silica rock coating in deserts; Kolb et al., 2004; Perry et al., 2006), in contrast to the gels formed somewhat later in the interior of the replaced sulfide grains. Such a formation of ''Si glues'' may have contributed to the good stability of first water contact gels (also in sulfate-rich, gel-poor environments; e.g. analysis X13 in Table 3) during subsequent mineral transformation reactions.

3.3.2.2. Gel-poor environments. Water circulation took place almost unhindered in generally coarser, less reactive material-rich and, subsequent to oxidative weathering, less gel-rich tailings using the remaining high active porosity. In contrast to above, the ''honeycombs'' were commonly partially filled only with jarosite-group minerals here, with or without crystalline Fe(III) oxyhydroxides present in addition. The jarosite covered surfaces of silicates, barite and fluorite also; it formed overgrowths on thin rims of Fe- or Si-rich allochthonous gels. The jarosite may have formed via precipitation from a supersaturated pore solution in decreasing pH conditions (e.g. Nordstrom, 1977; Dutrizac and Jambor, 2000), or by mixing of Fe–S-rich solutions from channels in the gel with K-rich pore solutions resulting from a somewhat later dissolution of aluminosilicates. A transformation of unstable (Si-poor; Fe-rich) S-poor gel into jarosite with a supply of K and S also can not be excluded.

3.4. Detailed characterization of cemented layers and hardpans

3.4.1. Types, mineralogical compositions and reduction of pore space by cementation

Cemented layers were gel-rich (bluish-grey colored) or moderately gel-bearing (mostly reddish-brown colored). Pale yellowish hardpans were not enriched in gels. A transitional type between cemented layers and hardpans, possibly cemented layers overprinted by precipitation of phases at the capillary fringe, was also reddish-brown colored. Interestingly, gel-rich cemented layers and hardpans were commonly found to occur in close spatial relationship (see discussion further down).

An example of an extremely gel-rich *cemented layer* was found in profile C (Fig. 6Aa), located in the sandy tailings close to the SE slope of the dam. Within an ~2 mm thin heavy mineral-rich layer, ~45% of Fe-rich secondary minerals including >30% of Fe–As–Si gels, were formed (Fig. 5a; Table 4). This gel-rich cemented layer is directly overlain by an essentially sulfide- and gel-free, gypsum-rich, jarosite-poor and ~2 mm thick hardpan with 16–27% of gypsum (Fig. 5c; Table 4).

The most important constraint on the remaining open pore space in the cemented layers is given by the amount of gel phases present; gels reduce the proportion of (connected) macro-pores much more efficiently than crystalline mineral phases in the studied samples. In the extreme case of profile C, the filled area was estimated to be ~99% in the gel-rich cemented layer (Table 4; Figs. 5a and 6Aa).

Hardpans were characterized by an enrichment in secondary gypsum and jarosite-group minerals making up from ~5 to sometimes >25% of the ROIs in studied thin sections (Tables 4 and 5; jarosite was attributed to the secondary Fe-rich phases). Gypsum occurred in anhedral aggregates or as crystals, whereas the jarosite-group minerals were microcrystalline, granular or formed micro-crusts.

The elevated concentrations of hydronium $(H_3O)^+$ in the jarosite-group minerals in sulfate-rich hardpans (Table 3; Fig. 7), as inferred from the analyzed low alkali contents in the minerals, indicate a generally low availability of Na and K during jarosite precipitation or may result from an extremely rapid weathering of the sulfides (e.g. Dutrizac and Jambor, 2000). In contrast, jarosite-group minerals, formed in interlaminated (a) mica-rich and (b) heavy mineral-rich layers and lenses (profile D – sequence (iii); Fig. 8d) are characterized by higher K and insignificant $(H_3O)^+$ concentrations (Table 3; Fig. 7). Small Fe(III) excess in the uncorrected jarosite formula probably results from an intergrowth of tiny grains of Fe(III) oxyhydroxides with the jarosite (corrected for analysis J20 in Table 3).

In contrast to gel-rich cemented layers, significant portions of partially filled pore areas (~12–>15%; edge agglutinated fragments/grains) and open pore areas (~3 to ~10%) were found for sulfate-rich hardpans without significant gel formation (e.g. profile E; Table 5; Fig. 6B).

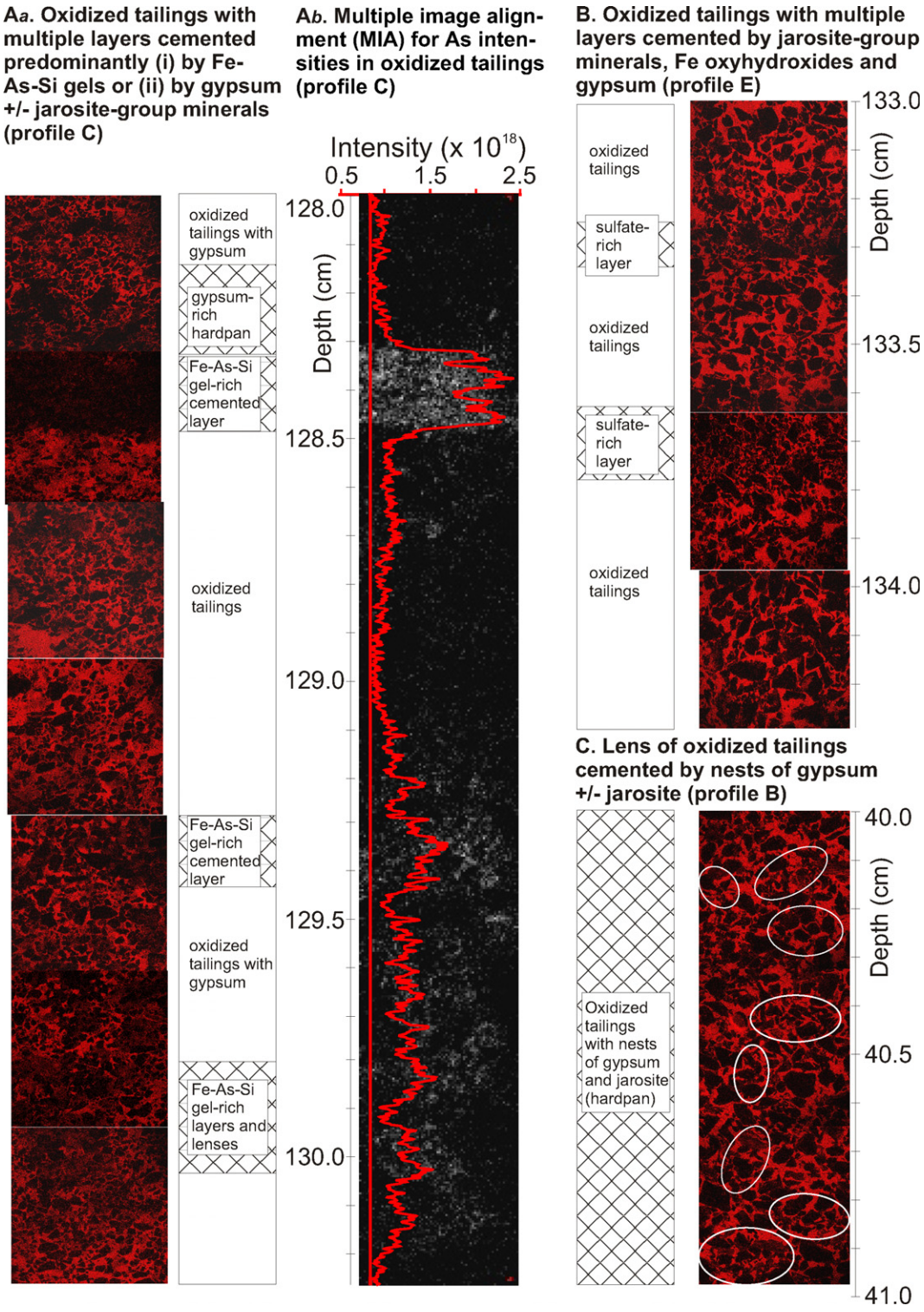

Fig. 6. (A)–(C) Results of the image processing for cemented layer/hardpan sequences from the sandy tailings within the Muenzbachtal tailings impoundment. Figures Aa, B and C show results of mapping for carbon (red), which is present in significant amounts in the embedding medium only (excluding small scale organic material). Therefore, it gives a good constraint on the distribution of filled, partially filled and open pores in the sediments. See text for details.

Table 4
Frequency distribution of primary and secondary mineral phases as well as of open and partially filled pores for profile C (depth: 128–130 cm) containing oxidized tailings, cemented layers and hardpans

Section/image	Filled area	Pore area		Primary mineral phases					Secondary mineral phases		Total[a]
		Partially filled	Open	Barite	Quartz	Silicates (excl. quartz)	Sulfides (pyrite)	Fluorite	Gypsum	Fe-rich phases (excl. sulfides)	
Oxidized tailings with gypsum/I-2	58.4	18.6	14.5	21.7	12.3	13.3	0.1	8.3	15.6	4.3	90.1
Gypsum-rich hardpan/I-2	80.6	12.1	3.3	18.7	12.7	15.3	0.2	2.6	27.0	4.1	83.9
Gel-rich cemented layer/I-1	99.2	0.6	<0.2	29.3	1.4	4.5	6.4	2.0	<0.1	46.2	89.8
Oxidized tailings/I-1	34.6	19.7	32.0	17.4	6.3	6.8	0.1	0.5	5.3	0.9	69.3
Oxidized tailings/I-3	55.8	17.6	17.0	21.9	13.7	9.5	1.2	1.2	7.1	5.7	77.3
Oxidized tailings/I-4	44.0	17.1	28.3	22.5	10.5	9.1	<0.1	0.7	0.7	8.5	80.3
Gel-rich cemented layer/I-5	72.6	11.9	10.2	26.3	5.8	15.2	1.1	2.0	0.7	27.8	89.1
Partialy cemented oxidized tailings/I-5	62.3	16.6	12.6	23.9	11.1	12.7	1.9	0.5	5.6	2.6	70.9
Gel-rich layers and lenses/I-6 and I-7	69.8	18.5	5.4	29.5	8.6	7.9	0.8	0.7	5.3	13.1	71.3
Oxidized tailings/I-7	41.5	21.3	25.0	32.1	8.4	6.7	0.1	3.0	0.7	5.5	81.5

Data from element distribution mapping – image processing technique; data in area%.
[a] Total was calculated from the area% of all minerals and of the open pore areas.

Table 5
Frequency distribution of primary and secondary mineral phases as well as of open and partially filled pores for profile E (depth: 133–134 cm) containing oxidized tailings and sulfate-rich hardpan layers

Section/image	Filled area	Pore area		Primary mineral phases				Secondary mineral phases		Total[a]
		Partially filled	Open	Barite	Quartz	Silicates (excl. quartz)	Fluorite	Gypsum	Fe-rich phases (excl. sulfides)	
Oxidized tailings/I-1	52.3	11.6	29.6	0.3	25.4	18.4	1.2	2.2	1.4	78.5
Sulfate-rich hardpan/I-1	75.0	12.2	7.0	2.3	15.8	38.8	4.8	4.7	17.3	90.7
Oxidized tailings/I-2	53.1	11.1	29.3	0.5	23.9	22.4	1.4	0.8	4.1	82.4
Sulfate-rich hardpan/I-3	68.6	15.2	9.9	2.7	13.8	24.7	3.2	4.4	20.1	78.8
Oxidized tailings/I-3	57.2	12.4	23.7	0.1	14.6	25.3	1.7	2.9	12.3	80.6
Oxidized tailings/I-4	65.5	10.5	18.3	1.8	23.8	26.1	1.2	4.3	4.7	80.2

Data from element distribution mapping – image processing technique; data in area%.
[a] Total was calculated from the area% of all minerals and of the open pore areas.

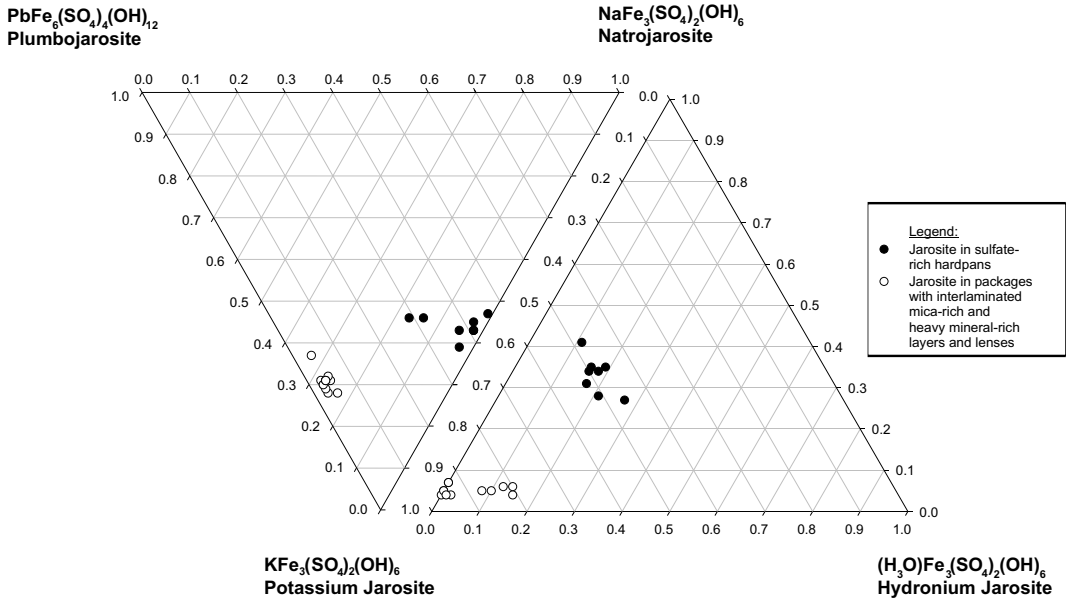

Fig. 7. Composition of jarosite-group minerals in different types of cemented layers/hardpans.

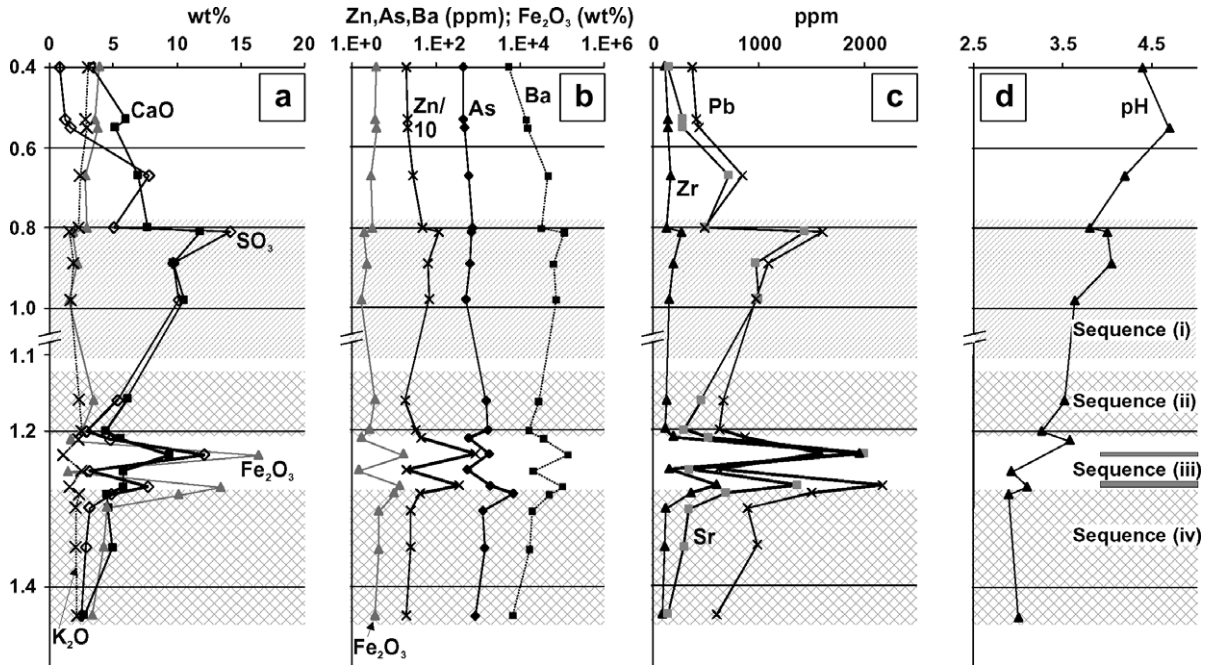

Fig. 8. (a)–(d) Geochemical profile (profile D) through a sequence of oxidized tailings with and without cementation by secondary phases. The measured pH values (paste pH) for the sediments are shown in (d).

3.4.2. Geochemical characterization

Fig. 8 shows the chemical composition of sandy tailings from profile D as a function of depth (Figs. 1a and 4). Fig. 8d illustrates that the paste pH values gradually decrease from top (pH ~4.5) to bottom (pH ~2.9) with their minimum in the reddish-brown sequences. The pH of the unaltered material at greater depth was ~6.4 to ~7.5 (this study and Jung, 2003). In profile D, four sequences are of special importance:

Sequence (i) is a pale-yellowish sequence of medium grained sand layers located at depths between ~0.8 and ~1.1 m. It consists of layers and lenses of variable thickness, which are either consolidated to hardpans or are unconsolidated. Sequence (i) is characterized by a strong enrichment in CaO, SO_3, Sr, Pb and Ba compared to the overlying, unconsolidated material. Microscopic analysis of thin sections indicated ~3 to ~5 area% of gypsum and ~3 to ~11 area% of secondary Fe-rich phases in the ROIs. Sulfur is predominantly bound in gypsum and barite. The high S values for this sequence cannot be generated by in situ oxidative weathering of Fe(II) sulfides only due to low Fe_2O_3 values; S was probably transported from oxidized sulfide-rich tailings (e.g. the underlying sequence (iii)).

Sequence (ii) is a strongly consolidated dark reddish-brown sequence (transitional type of consolidated layer; see Section 3.4.1) of predominantly medium grained sands at depths between ~1.1 and ~1.2 m. It is characterized by higher Fe_2O_3 and As concentrations, but significantly lower CaO, SO_3, Sr and Pb values compared to sequence (i). These data suggest a lower abundance of gypsum and a higher abundance of secondary Fe(III)-rich phases compared to sequence (i). This sequence thins out at locations where the underlying sequence (iii) is missing.

Sequence (iii) consists of interlaminated sand/silt layers of dark grey sand and pale-yellowish silt at depths between 1.21 and 1.27 m. The silt layers were $\leqslant$1 mm thick. These layers were weakly agglutinated in the field, however, drying resulted in their consolidation, which is explained by precipitation of euhedral gypsum. Sequence (iii) is characterized either by strong enrichment in Fe_2O_3, SO_3, Zn, As, Ba, Zr, Pb and Sr in the thin greyish layers, or by increased K_2O and CaO, but relatively low Fe_2O_3 values, in the pale yellowish silt layers. These data are consistent with petrographic and XRD results, which indicate heavy mineral enrichment (e.g. barite, zircon, pyrite) in the sand layers, and increased concentrations of aluminosilicates (micas $\pm$ Ca-bearing plagioclase) in the silt layers. Sequence (iii) shows a low occurrence of Fe–As–Si-rich gels and a high enrichment in Fe hydroxysulfates. Large aggregates of jarosite-group minerals occurred in bended layers outlining the weathered sheet structure of the replaced micas. They also occurred in interstitials between mineral grains or inside scarce "honeycombs" in these layers.

Sequence (iv) is another strongly consolidated dark reddish-brown sequence (transitional type), which occurs at depths between ~1.3 and at least 1.5 m. This sequence is very similar in appearance to sequence (ii).

3.4.3. Metal sulfide oxidizing microorganisms

Cell numbers of Fe-oxidizing and S-oxidizing microorganisms were investigated at different depths in profile A (Fig. 3E). A pronounced change in cell numbers of metal sulfide oxidizing bacteria in accordance with lithology was observed. Cell numbers were between 10^4 and 10^7 cells/g dry weight (dw) in the zone of oxidized tailings, while they increased to 10^9 cells/g dw below the upper cemented layer in the sulfide-bearing zone. The relatively low cell numbers for the upper cemented layer may be explained by the remaining relatively low sulfide content of this layer (Fig. 3C), and probably indicates a downward movement of the oxidation front with time. Cell numbers remained at high levels down to ~1 m, and decreased in the deepest grey silt layer. Cell numbers of acidophilic Fe(II)-oxidizing microorganisms (*A. ferrooxidans*-like bacteria) were generally higher than those of acidophilic S-oxidizing microorganisms (*Acidithiobacillus thiooxidans*-like bacteria), except for depths below ~1 m. The maximum numbers of Fe-oxidizing microorganisms are among the highest detected in sulfidic tailings (Southam and Beveridge, 1992; Blowes et al., 1998; Diaby et al., 2007).

In the oxidized zone of the sandy tailings, cell numbers for Fe(II)-oxidizing microorganisms (maximum value: ~10^7 cells /g dw) were distinctly lower than measured for profile A in the slimes area. The only location with significant numbers of living cells up to 10^7 cells/g dw (*A. ferrooxidans*) was a grey silt layer underlying a cemented package of sandy material (data not shown).

3.4.4. Geophysical characterization

Profile A was studied by 11 SIP measurements at different depths (Fig. 3A and B). The amplitude of resistivity shows a continuous decrease due to increasing water contents, which is intensified by decreasing grain sizes. The shapes of the phase spectra at 2.9 and 750 Hz showed a remarkable change at the position of the cemented layers. This corresponds to a change in sulfide content in the same depth range (Fig. 3C). The spectral electrical data indicate another change at a depth of ~0.7 m, which cannot be explained by the similar sulfide contents

over the depth range ~0.65 to ~1.0 m; however, it could be related to increased surface areas of the sulfides in the narrow zone from ~0.65 to ~0.70 m as a result of strong oxidative weathering.

The outcrops in the sandy tailings (e.g. profile D; Fig. 4), did not show any change in the phase spectra patterns. All measured phase angles are lower than 10 mrad over the total measured frequency range (results not shown). This finding is consistent with the fact that these outcrops are located completely in the strongly weathered zone (essentially no sulfides present).

3.5. Simplified model for cemented layer and hardpan formation in the Muenzbachtal tailings impoundment

The extent of cemented layer and hardpan formation in mine tailings primarily depends on (i) the amount of reactive materials present and their accessible surface areas (selective dissolution of phases or particles during alteration might enhance the reactive surface area up to a factor of 10,000; Rammlmair, 2002), (ii) the presence of relatively impervious layers in direct proximity of the reactive phases, and (iii) mass transport processes that allow selective leaching of reactive phases from one layer and agglutination of mineral grains in another layer. The evolution of micro-porosity and micro-channels due to selective leaching of reactive phases (e.g. Rammlmair, 2002) and agglutination of mineral grains plays a key role in mass transport and precipitation processes.

Cemented layers occurred in originally reactive material-rich heavy mineral layers overlying fine-grained weathered silt layers or related to interlaminated reactive material-rich sequences, suggesting a genetic relationship between these layers during weathering. A simplified model for the formation of the sequence of cemented layers and hardpans as typically found in the Muenzbachtal tailings impoundment is outlined in Fig. 9 and discussed in detail below.

Fig. 9(1) shows a typical sequence of layers before weathering. From top to bottom can be recognised: fine to medium grained sands, a heavy mineral-rich layer, a silt layer, followed by multiple interlaminated sand and silt layers. The major primary reactive phases within the heavy mineral-rich layer are sulfides, which were the main sources of S, Fe, As, Zn and Pb. Within the silt layers, the main reactive mineral in addition to the sulfides is biotite, which is a major source of K, Fe, and Si. The main Ca source is Ca-bearing plagioclase (cf. Bhatti et al., 1994), which occurs in the sand layers, and in the silt layers as well, but in lower concentrations. Mineral processing solutions contained Ca hydroxide and minor Ca hypochlorite, which may, to a small degree, have also been deposited in the tailings impoundment. A re-dissolution of highly soluble secondary phases could be considered as a source of elements as well.

The most significant weathering process is the oxidation of metal sulfides, which produces large amounts of sulfuric acid and mobile Fe(II). Eqs.

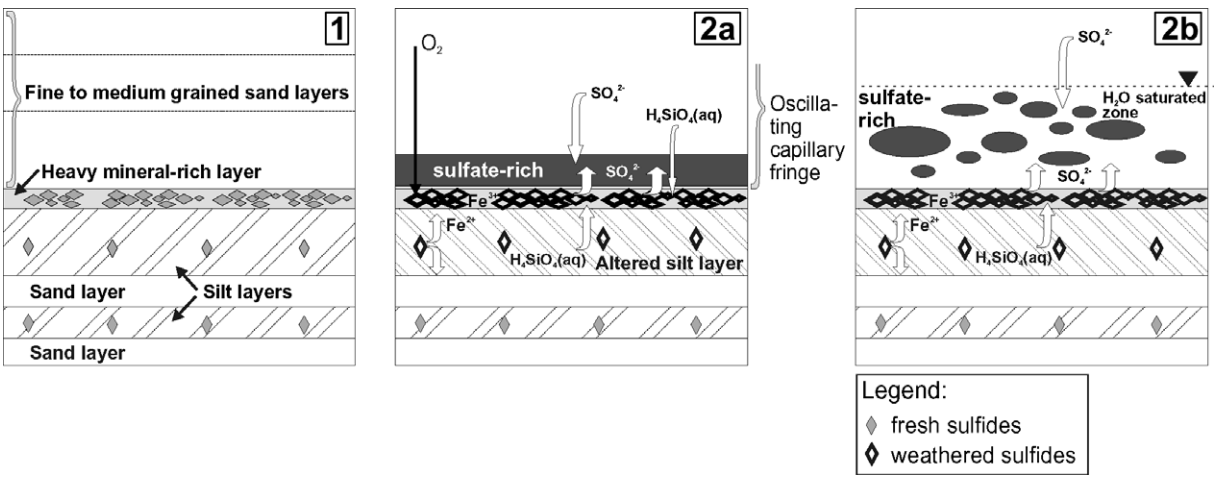

Fig. 9. Simplified model for formation of hardpan sequences within the tailings impoundment Muenzbachtal. (1) Schematic profile before weathering of tailings material. (2a and b). Profiles after weathering of reactive phases and formation of gel-rich (light grey) and gel-poor (dark grey) cemented layers and hardpans. See text for further details.

(1)–(4) may characterize the oxidation of arsenopyrite, which is a very complicated process involving many individual reaction steps. Reactions (1), (2) and (4) are usually bacterially mediated (e.g. Tuovinen et al., 1994; Morin and Calas, 2006).

$$FeAsS_{(s)} + 11/4O_2 + 3/2H_2O \Longleftrightarrow Fe^{2+} + SO_4^{2-} + H_3AsO_3 \quad (1)$$

$$Fe^{2+} + 1/4O_2 + H^+ \Rightarrow Fe^{3+} + 1/2\ H_2O \quad (2)$$

$$Fe^{3+} + 3H_2O \Longleftrightarrow Fe(OH)_{3(s)} + 3H^+ \quad (3)$$

$$H_3AsO_3 + 1/2O_2 \Longleftrightarrow H_2AsO_4^- + H^+ \quad (4)$$

Iron- and S-oxidizing microorganisms have been shown to play a significant role in catalyzing these reactions (Fig. 3). Field eluates prepared from cemented heavy mineral-rich layers and underlying silt layers (profile A) yielded pH values between 2.5 and 4.0 and dissolved Fe(II) concentrations up to ~250 mg/L. These conditions allow transport of Fe and SO_4 towards the redox interface between the reduced silt on the one hand, and the water-unsaturated sand layers on the other hand (Fig. 9(2a)). Subsequent oxidation of Fe(II) to Fe(III) leads to the precipitation of amorphous Fe-oxyhydroxides at this interface (Eqs. (2 and 3)). Increased oxidation of As(III), formed by arsenopyrite oxidation (Eq. (1)), to As(V), was observed in experiments with increased Fe(III) concentrations (Yunmei et al., 2004). However, As(III) oxidation (Eq. (4)) may also be catalyzed by microorgansims, e.g. *Thiomonas* sp. (Bruneel et al., 2003; Morin and Calas, 2006). The low As(III)/As(V) ratios (0.03 to mostly $\leqslant$0.11; only one value of 0.19) found for the oxidized or partly oxidized tailings materials in profile A (Fig. 3) may, therefore, indicate an increased activity of the aforementioned bacteria for arsenite oxidation at this location.

In micro-domains, the released acid (Eqs. (3) and (4)) may result in lower pH values than measured for the bulk material (pH ~ 2.5). In sulphide-rich micro-domains, pH values <1 were measured in biofilms (Vlasceanu et al., 2000). Under these conditions aluminosilicates like mica and plagioclase would become increasingly unstable, causing a stronger release of Si, Al, K, Ca and F into the pore solutions (e.g. Blum and Stillings, 1995), but also resulting in an effective buffering of the pH. Precipitation of Fe(III) phases would take place in adjacent sand or silt layers in the case that the sulphide-rich layers are poor in aluminosilicates.

The initial precipitates after oxidative weathering processes, which cover the surfaces of the weathered minerals and of adjacent sand grains, are usually poorly crystalline (gel-like) because such phases have lower interfacial free energies than more crystalline products (Steefel and van Cappellen, 1990). These covers may also include portions of extra-cellular polymeric substances (EPS) produced by the Fe-oxidizing bacteria (e.g. Schultze-Lam et al., 1996; Gehrke et al., 1998; Sand et al., 2001; Harneit et al., 2006) with accumulated metals (e.g. Fe(III) complexes). The amounts of EPS as produced by growth of one strain of *A. ferrooxidans* on pyrite was 2.76 mg per 10^{10} cells (Gehrke et al., 1998). Assuming that the Fe-oxidizing bacteria produce an equal amount of EPS in nature, the concentration of EPS would be considerable (~0.3 mg/g dw) at the oxidation front of the tailings material in profile A (where 10^9 cells/g dw were detected; Fig. 3E). The initial precipitates are expected to be composed of Fe(III) oxyhydroxides and hydroxysulfates with significant H_2O, adsorbed As and Ca, as well as Si at strongly varying concentrations. Subsequent drying would result in the formation of stable Fe–Si cemented layers by loss of water molecules. Furthermore, Si-dominated gels were observed as thin coatings on mineral grains in oxidized mine tailings.

Fig. 9(2a) shows the generation of a sulfate-rich hardpan overlying the gel-rich cemented layer. This hardpan mainly consists of gypsum and jarosite-group minerals, and is essentially gel-poor. Under influence of oscillating capillary fringes on top of the semi-impermeable cemented layer, transport of significant portions of SO_4 from the layers with intense sulfide oxidation into the hanging sulfide-poor, intermediate-grained sand layers, has to be assumed. Additional sources of SO_4 are the overlying oxidized sand layers. From mineralogical observations it is inferred that the gypsum-rich hardpans were mainly formed somewhat later than the gel-rich cemented layers (in a continuous process). This inference is in agreement with the experimental data of Bhatti et al. (1994), who explained a similar observation by a retarded release of Ca from the plagioclase feldspar in his experiments. Under special conditions, i.e. the formation of basins with widely oscillating capillary fringes and the formation of preferential solution pathways in the sandy matrix on top of semi-impermeable silt/clay layers, gypsum will not precipitate in continuous layers, but in irregularly distributed nests over a much wider cemented zone (Fig. 9(2b)).

After completion of the weathering processes, the topmost greyish, sulfide-bearing silt/clay layer has been transformed into a bleached, sulfide-free and clay-mineral enriched silt layer, overlain by a cemented heavy mineral-rich layer with agglutinating Fe(III) oxyhydroxide-silicate coatings. The interface between this cemented layer and the coarser-grained, water-unsaturated sand layer acts as a contact surface for dissolved O_2. A sulfate-rich hardpan that has formed somewhat higher in the profile, completes the typical sequence.

3.6. Contaminant attenuation adherence in oxidized mine tailings

Contaminants that may pose serious pollution threats to the water systems at the Muenzbachtal site are mainly As, Zn and Pb. Table 3 displays the concentrations of contaminants and major elements in jarosite-group minerals and poorly crystalline phases collected from hardpans and cemented layers from the Muenzbachtal site. Contaminant concentrations in gypsum were below the limit of detection (LOD) for both gypsum-rich hardpans and cemented layers.

Zinc concentrations were below the LOD in analysed secondary minerals and gels. Zinc was not fixed effectively in the precipitated secondary mineral phases and was lost in large parts to the groundwater. Data of Martin et al. (1994) confirm a similar scenario for the oxidative weathering of sulfides from the Freiberg mine workings and estimates its contribution to the Zn load of the Elbe river to be ~30%.

Table 3 shows that the analyzed crystals of jarosite-group minerals always contained As and Pb. Jarosite-group minerals may act as a sink for trace elements by adsorption/substitution/co-precipitation processes (e.g. Scott, 1987; McGregor and Blowes, 2002). Lead probably substitutes for K (Dutrizac and Jambor, 2000) and AsO_4^{3-} for SO_4^{2-} in the jarosite structure (Paktunc and Dutrizac, 2003). All analysed jarosite-group mineral grains from packages with mica- and heavy mineral-rich layers (profile D – sequence (iii); Fig. 8; analyses J34–J40 in Table 3) contained significantly higher Pb and As concentrations than the studied grains (analyses J19–J24 in Table 3) derived from sulfate-rich hardpans.

The highest As concentrations were found in gel phases (Table 3). The As and Pb concentrations in gels from the extremely gel-rich cemented layer in profile C were always significantly higher (by a factor of >10 for As) than in gels from sulfate-rich and gel-poor hardpans. The high As/Fe mole ratios (>0.15) support formation of FeOHAs (amorphous/poorly crystalline Fe(III) hydroxy arsenate) minerals (e.g. Carlson et al., 2002; Morin et al., 2003). These poorly crystalline Fe–As-rich phases contain significantly lower S concentrations than the jarosite-group minerals and would have chemical formulas that are rather variable (commonly with SiO_2 contents; Table 3) and different from that of schwertmannite ($Fe_8O_8(OH)_6SO_4 \cdot nH_2O$; e.g. Murad et al., 1994). However, the presence of portions of schwertmannite in the gel rims would not contradict the measured pH conditions in the zones with hardpan formation (pH: ~3 or slightly lower), which fit well with the experimental determined formation conditions for schwertmannite (pH: ~3; e.g. Bigham and Nordstrom, 2000). Furthermore, XRD or EM analysis did not indicate a high abundance of scorodite or of similar Fe(III) arsenate precipitates to be intergrown with the gel at the Muenzbachtal site, despite pH conditions which fit the range for precipitation of poorly crystalline scorodite as found by Langmuir et al. (2006; pH 2–3). Goethite could also not be observed using XRD.

In Table 3, the As and S concentrations of the gels were normalized to the stoichiometric composition of arsenopyrite. This procedure is justified by the shapes of the measured gel aggregates in the gel-rich cemented layer; these clearly confirm arsenopyrite as the main sulfide replaced here. The results of the calculation show that the As loss from the solids to the migrating pore water during oxidative weathering of the sulfides was between <20% and 30%, whereas the loss of S seems to be much higher (~90%). However, portions of the S are present as accumulated native S in the central parts of the replaced grains. In sulfate-rich hardpans, the estimated As loss from the oxidized sulfides to the migrating pore water could have been higher (up to 95%) than at gel-rich locations, and maybe similar to the estimated values for the S loss (data for first contact gels from "honeycomb-like" textures – see Table 3).

The contents of Zn, As and Pb in the dam pore waters and sediment components were determined by sequential extractions. Fig. 3G shows the contaminant and Fe amounts extracted from profile A (Fig. 3F) sediment samples. The bars indicate the amounts as extracted in the individual extraction

steps (Table 1) as well as the total sediment contents (compare also the lines in Fig. 3F).

Zinc is the only pollutant with significant dissolved and cation exchangeable fractions (fractions I and II), while Zn amounts bound to Fe oxyhydroxides are low when compared to As and Pb (fractions VI and VII). In layers where readily oxidizable Zn sulfides are still present (step VIII; samples d1, e and f), the total Zn contents of the sediments rise by factors of >2. Additionally, the presence of inclusions of Zn phases (probably sphalerite) in e.g. silicates is indicated for all profile A samples by the step IX data (Fig. 3G).

Lead was extracted from organic bonds (step V), poorly crystalline Fe oxyhydroxides, jarosite-group minerals and gels (step VI), crystalline Fe oxides and jarosites (step VII), readily oxidizable Pb sulfides (step VIII; samples e and f) and from oxidation products of galena or Pb phases (probably galena) enclosed in silicates (step IX). In contrast to Zn, the Pb released during extraction step IX accounts for almost half of the total Pb content of the sediments. Except for samples e and f (presence of readily oxidizable Pb sulfides), poorly crystalline Fe phases contain about half of the total sediment Pb.

Arsenic sediment contents show their highest values in the cemented layers (samples b, d1, d2), where poorly crystalline Fe phases (predominantly gels; see Table 3) are the only As-bearing fraction (step VI). In all other samples, minor As amounts were additionally extracted in step V (probably deriving from hydrated gels). Samples e and f contain As bound to sulfide inclusions in silicates (arsenopyrite).

Contaminant attenuation in the oxidized zones is related to their retention at the cation exchange complex (1–3% Zn saturation) and to their adsorption/incorporation on/in poorly-crystalline Fe oxyhydroxides (Zn occupation of high affinity cation sorption sites), jarosites (Pb–K and AsO_4–SO_4 substitutions) and gels (AsO_4 and Pb incorporation) as well as on crystalline Fe oxides (As sorption at non-specific sorption sites) and jarosites (Pb–K substitution). Reverse calculations from secondary mineral phase compositions (Table 3) and elemental concentrations of the extraction solutions VI and VII (cf. Table 1) reveal dehydrated gels to be the predominant As carriers, while jarosites contain most of the Pb. Zinc retention in Fe oxyhydroxides relies on sorption in high affinity cation sorption sites and is limited by the amount of those sites (Dzombak and Morel, 1990).

4. Summary and environmental implications

The studied tailings impoundment is characterized by an intense mineralogical and textural reorganization of the heaped material in its uppermost oxidized zone. The oxidation of sulfide-rich and underlying silt layers catalyzed by bacterial activity has resulted in the formation of characteristic sequences of gel-rich and gel-poor cemented layers and overlying hardpans in the depths range 0.3 to ~1.5 m. Thick gel-poor hardpans characterized by edge agglutinated fragments (cf. Rammlmair, 2002) are frequent in the oxidized zone of the sandy tailings.

The occurrence and abundance of hardpans in oxidized tailings depends primarily on the amount of available reactive materials. It is concluded from the data that a heterogeneous distribution of the reactive minerals with strong enrichment in sulfides in heavy mineral-rich layers, and in aluminosilicates in adjacent silt layers, as well as their location with respect to the water table, may be a very important constraint for effective cemented layer and hardpan formation at a given site. Micro-domains with development of extreme pH and pe conditions and formation of Redox interfaces triggered by the heterogeneity of the heaped material result in an effective formation of sequences with gel- and sulfate-rich cemented layers and hardpans with a high potential for natural attenuation of As, Pb and other contaminants.

High resolution profiling carried out in this study shows that the dramatic change in cell numbers of microorganisms (i.e. *A. ferrooxidans*) at the recent position of the oxidation front, which is also defined by the strong changes in the geophysical and geochemical data, clearly coincides with the location of the cemented layer – hardpan sequences (Fig. 3). This highlights the importance of biogeochemical processes not only for the mediation of metal sulfide oxidation, but also for cemented layer formation. The surface of the cells itself or their EPS consisting of organic C with complexed metals (Sand et al., 2001) may have served as nucleation sites for secondary mineral formation (e.g. Ferris et al., 1989; Southam and Beveridge, 1992).

Hardpans in mine tailings have been suggested to have a number of important effects especially in minimizing the discharge of toxic substances from the heaped material (e.g. McGregor and Blowes, 2002; Rammlmair, 2002; Gilbert et al., 2003). Formation of dense hardpans at the surface of the heap

by agglutination of sediment with gels in a multi-step process (cf. Rammlmair, 2002), which would primarily result in an encapsulation of significant cells of the mine tailings materials, and thus reducing infiltration of rain water and lessen the rate of sulfide oxidation, did not occur at the studied location. The lateral transport at the slightly inclined layers towards the centre of the heap might play a role for the immediate vicinity, but is not significant for the whole dam system at Freiberg. However, the gel-rich cemented layers with remaining low porosities in conjunction with associated silt/clay layers seem to have been rather effective locally in slowing down the downward movement of the oxidation front in the studied parts of the tailings impoundment.

The main effect of the cemented layer–hardpan sequences at the Muenzbachtal site is the, at least temporary, natural attenuation of the toxic As and Pb species in the formed secondary phases. The data show that (i) there is an extreme decrease in the occurrence of As-bearing phases at the margins of Fe–As–Si gel-rich cemented layers (Fig. 6Ab; MIA data from image processing). This indicates only small As losses from these originally highly As sulfide-bearing layers subsequent to sulfide oxidation and is reflected in a limited incorporation in secondary As phases within the under- or overlying sediments. This interpretation is consistent with (ii) the microchemistry of the Fe–As–Si-gel phases in gel-rich hardpans (Table 3 and discussion) and the calculated relatively small As losses during sulfide weathering and subsequent gel formation in these layers. Arsenic enrichment in cemented layers is caused by its incorporation in dehydrated gels, which act as cementing agent and show distinct enrichment in cemented layers. In neutral and basic environments, Fe(III) arsenate compounds having Fe/As molar ratios <4 are less thermodynamically stable than those with higher ratios (Robins, 1987; Krause and Ettel, 1989; Paktunc et al., 2004). However, it is assumed that the Fe–As–Si gels are stabilized by the developed Si networks with polyvalent cations in these phases.

Jarosite-group minerals cementing sediments close to heavy mineral-rich layers were also capable of incorporating significant amounts of As and particularly Pb (see Table 3 and discussion). The stability of jarosite-group minerals is good in the acidic environment; however, they become unstable at pH >5 (replacement by goethite; McGregor and Blowes, 2002) with loss of K^+, SO_4^{2-}, H^+ and, at least, some of the AsO_4^{3-} and Pb^{2+} to the solution. On the other hand, the freshly formed Fe oxyhydroxides would provide reactive sites for sorption of both anions (e.g. AsO_4^{3-}) and cations (e.g. Pb^{2+}). Their points of zero charge range from pH 6 to 10 (Cornell and Schwertmann, 2003), suggesting both negative and positive surface charges at $pH > 5$. Additionally, Fe oxyhydroxides possess high affinity cation sorption sites, which preferentially bind Zn^{2+} (formation of inner sphere complexes). Thus, Zn retention would also increase with increasing sediment amounts of Fe oxyhydroxides.

However, for the material present in the oxidized zone of the studied tailings impoundment, such strong geochemical changes are not likely for the near future. Under the given environmental conditions, Zn is extensively mobilized by oxidation of primary Zn sulfides. Zinc retention at the cation exchange complex (clay minerals, micas) and in Fe oxyhydroxides is small compared to sulfidic Zn contents of anoxic sediment zones. Zinc is not effectively retarded in the oxidized zone and subject to translocation. In contrast, Pb and As from sulfidic minerals are mobilized to a much smaller extent during oxidation since they undergo retardation in minerals of the oxidation zone. Whilst jarosites are more or less present in the whole oxidized zone, dehydrated gels are considerably enriched in the cemented layers.

The gel-poor and sulfate-rich hardpans (especially gypsum), which are strongly developed at the slopes of the tailings impoundment, are important in preventing the tailings from deep erosion. These hardpans are only temporarily stable; however, their dissolution results only in Ca^{2+} and SO_4^{2-} release to the pore water due to the lack of toxic substances in the dominating gypsum. Since pore waters are widely in equilibrium with gypsum, cation exchange and sorption equilibria would not be affected much.

Acknowledgements

The authors are grateful to SAXONIA Standortentwicklungs- und -verwaltungs gesellschaft mbH (Freiberg, Germany), who allowed us to conduct investigations on their property. We particularly thank Dr. Mollée for his support of the field work. Technical assistance of J. Lodziak (BGR Hannover) during microprobe work is appreciated. The authors are grateful to S. Kaufhold and D. Weck

(BGR Hannover) for X-ray diffraction analysis of mine tailings. N. Abraham and F. Korte (BGR Hannover) are thanked for analytical work. The project was financed by grant 0330523 provided by the Bundesministerium fuer Bildung und Forschung (PT Jülich) of Germany. The authors also thank D. Paktunc and M. Tichomirowa for their critical comments which significantly improved the manuscript.

References

Agro-consult Dresden (ACD) GmbH, 1993. Historical research on the landed property of the SAXONIA AG, Freiberg; Part 2. The Muenzbachtal tailings impoundment, Freiberg. Unpublished report, University of Freiberg, Freiberg, Saxony, Germany.

Archie, G.E., 1942. The electrical resistivity log as an aid in determining some reservoir characteristics. Trans. Am. Inst., Met. Petr. Eng. 146, 54–62.

Bhatti, T.M., Bigham, J.M., Vourinen, A., Tuovinen, O.H., 1994. Alteration of mica and feldspar associated with the microbiological oxidation of pyrrhotite and pyrite. In: Alpers, C.N., Blowes, D.W. (Eds.), Environmental Geochemistry and Sulfide Oxidation. ACS Symposium Series 550, Washington, USA, pp. 90–105.

Bigham, J.M., Nordstrom, D.K., 2000. Iron and aluminum hydroxysulfates from acid sulfate waters. In: Alpers, C.N., Jambor, J.L., Nordstrom, D.K. (Eds.), Sulfate Minerals: Crystallography, Geochemistry, and Environmental Significance, Rev. Mineral. Geochem. 40, Washington, USA, pp. 351–403.

Blowes, D.W., Jambor, J.L., 1990. The pore-water chemistry and the mineralogy of the vadose zone of sulfide tailings, Waite Amulet, Quebec. Appl. Geochem. 5, 327–346.

Blowes, D.W., Jambor, J.L., Hanton-Fong, C.J., Lortie, L., Gould, W.D., 1998. Geochemical, mineralogical and microbiological characterization of a sulfide-bearing carbonate-rich gold-mine tailings impoundment, Joutel, Québec. Appl. Geochem. 13, 687–705.

Blowes, D.W., Ptacek, C.J., Jambor, J.L., Weisner, C.G., 2005. The geochemistry of acid mine drainage. In: Sherwood Lollar, B. (Ed.), Environmental Geochemistry, Treatise on Geochemistry, vol. 9. Elsevier, Amsterdam, pp. 150–204.

Blum, A.E., Stillings, L.L., 1995. Feldspar dissolution kinetics. In: White, A.F., Brantley, S.L. (Eds.), Chemical Weathering Rates of Silicate Minerals, Reviews in Mineralogy, vol. 31. Mineralogical Society of America, Washington, pp. 291–351.

Bruneel, O., Personne, J.C., Casiot, C., Leblanc, M., Elbaz-Poulichet, F., Mahler, B.J., Le Fleche, A., Grimont, P.A.D., 2003. Mediation of arsenic oxidation by *Thiomonas* sp. in acid-mine drainage (Carnoules, France). J. Appl. Microbiol. 95, 492–499.

Carlson, L., Bigham, J.M., Schwertmann, U., Kyek, A., Wagner, F., 2002. Scavenging of As from acid mine drainage by schwertmannite and ferrihydrite: a comparison with synthetic analogues. Environ. Sci. Technol. 36, 1712–1719.

Cochran, W.G., 1950. Estimation of bacterial densities by means of the "most probable number". Biometrics 6, 105–196.

Coggans, C.J., Blowes, D.W., Robertson, W.D., Jambor, J.L., 1999. The hydrogeochemistry of a nickel-mine tailings impoundment – Copper Cliff, Ontario. In: Filipek, L.H., Plumlee, G.S. (Eds.), The Environmental Geochemistry of Mineral Deposits, Part B: Case Studies and Research Topics. Rev. Econ. Geol. vol. 6B, pp. 447–465.

Cornell, R.M., Schwertmann, U., 2003. The Iron Oxides. Wiley–VCH Verlag, Weinheim.

Courtin-Nomade, A., Bril, H., Neel, C., Lenain, J., 2003. Arsenic in iron cements developed within tailings of a former metalliferous mine – Enguiales, Aveyron, France. Appl. Geochem. 18, 395–408.

Diaby, N., Dold, B., Pfeifer, H.R., Hollinger, C., Barrie Johnson, D., Hallberg, K.B., 2007. Microbial communities in a porphyry copper tailings impoundment and their impact on the geochemical dynamics of the mine waste. Environ. Microbiol. 9, 298–307.

Dold, B., 2003. Speciation of the most soluble phases in a sequential extraction procedure adapted for geochemical studies of copper sulfide mine waste. J. Geochem. Explor. 80, 55–68.

Dutrizac, J.E., Jambor, J.L., 2000. Jarosites and their application in hydrometallurgy. In: Alpers, C.N., Jambor, J.L., Nordstrom, D.K. (Eds.), Sulfate Minerals: Crystallography, Geochemistry, and Environmental Significance, Rev. Mineral. Geochem. 40, Washington, USA, pp. 405–452.

Dzombak, D.A., Morel, F.M.M., 1990. Surface Complexation Modelling: Hydrous Ferric Oxide. John Wiley, New York, USA.

Ehrlich, H.L., 2002. Geomicrobiology. Marcel Dekker AG, New York, USA.

Ferris, F.G., Schultze, S., Witten, T.C., Fyfe, W.S., Beveridge, T.J., 1989. Metal interactions with microbial biofilms in acidic and neutral pH environments. Appl. Environ. Microbiol. 55, 1249–1257.

Furche, M., Meima, J.A., Graupner, T., Grissemann, Ch., Rammlmair, D., 2007. Transport in mine tailings: Geophysical monitoring and reactive transport modelling. In: Proceedings of SGA Meeting 2007, Dublin, Ireland.

Gault, A.G., Cooke, D.R., Townsend, A.T., Charnock, J.M., Polya, D.A., 2005. Mechanisms of arsenic attenuation in acid mine drainage from Mount Bischoff, western Tasmania. Sci. Total Environ. 345, 219–228.

Gehrke, T., Telegdi, J., Thierry, D., Sand, W., 1998. Importance of extracellular polymeric substances from *Thiobacillus ferrooxidans* for bioleaching. Appl. Environ. Microbiol. 64, 2743–2747.

Giere, N.V., Sidenko, E.V., Lazareva, E.V., 2003. The role of secondary minerals in controlling the migration of arsenic and metals from high-sulfide wastes (Berikul gold mine, Siberia). Appl. Geochem. 18, 1347–1359.

Gilbert, S.E., Cooke, D.R., Hollings, P., 2003. The effects of hardpan layers on the water chemistry from the leaching of pyrrhotite-rich tailings material. Environ. Geol. 44, 687–697.

Gunsinger, M.R., Ptacek, C.J., Blowes, D.W., Jambor, J.L., 2006. Evaluation of long-term sulfide oxidation processes within pyrrhotite-rich tailings, Lynn Lake, Manitoba. J. Contam. Hydrol. 83, 149–170.

Harneit, K., Göksel, A., Kock, D., Klock, J.-H., Gehrke, T., Sand, W., 2006. Adhesion to metal sulfide surfaces by cells of *Acidithiobacillus ferrooxidans*, *Acidithiobacillus thiooxidans*

and *Leptospirillum ferrooxidans*. Hydrometallurgy 93, 245–254.

Haubrich, F., Baake, D., Kluge, A., Kindermann, A., Winkler, C., 2000. Weathering of sulfides in mined ore veins. A field of complex geochemical–mineralogical research. In: Wippermann, T. (Ed.), Bergbau und Umwelt. Springer–Verlag, pp. 57–66, in German.

Johnson, R.H., Blowes, D.W., Robertson, W.D., Jambor, J.L., 2000. The hydrogeochemistry of the nickel rim mine tailings impoundment, Sudbury, Ontario. J. Contam. Hydrol. 41, 49–80.

Jung, H.G., 2003. Secondary processes in mine dumps and tailings impoundments – control on metal mobility and hardpan formation. Unpublished PhD thesis, Marburg University, Germany.

Kolb, V.M., Philip, A.I., Perry, R.S., 2004. Testing the role of silicic acid and bioorganic materials in the formation of desert varnish. In: Hoover, R.B., Levin, G.V., Rozanov, A.Y. (Eds.), Instruments, Methods, and Missions for Astrobiology VIII, Proceedings of SPIE, vol. 5555, pp. 116–125.

Korte, N.C., Fernando, Q., 1991. A review of arsenic(III) in groundwater. Crit. Rev. Environ. Control 21, 1–39.

Krause, E., Ettel, V.A., 1989. Solubilities and stabilities of ferric arsenates. Hydrometrics 22, 311–337.

Langmuir, D., Mahoney, J., Rowson, J., 2006. Solubility products of amorphous ferric arsenate and crystalline scorodite ($FeAsO_4 \cdot 2H_2O$) and their application to arsenic behavior in buried mine tailings. Geochim. Cosmochim. Acta 70, 2942–2956.

Leathen, W.W., McIntyre, L.D., Braley, S.A., 1951. A medium for the study of bacterial oxidation of ferrous iron. Science 114, 280–281.

Martin, M., Beuge, P., Kluge, A., Hoppe, T., 1994. Mine drainage waters of the ore mountains – source of the heavy metal load of the Elbe river. Spektrum der Wissensch. 5, 102–107, in German.

McGregor, R.G., Blowes, D.W., 2002. The physical, chemical and mineralogical properties of three cemented layers within sulfide-bearing mine tailings. J. Geochem. Explor. 76, 195–207.

Moncur, M.C., Ptacek, C.J., Blowes, D.W., Jambor, J.L., 2005. Release, transport and attenuation of metals from an old tailings impoundment. Appl. Geochem. 20, 639–659.

Morin, G., Calas, G., 2006. Arsenic in soils, mine tailings, and former industrial sites. Elements 2, 97–101.

Morin, G., Juillot, F., Casiot, C., Bruneel, O., Personne, J.C., Elbaz-Poulichet, F., Leblanc, M., Ildefonse, P., Calas, G., 2003. Bacterial formation of tooeleite and mixed arsenic(III) or arsenic(V)–iron(III) gels in the Carnoules acid mine drainage, France. Environ. Sci. Technol. 37, 1705–1712.

Murad, E., Schwertmann, U., Bigham, J.M., Carlson, L., 1994. Mineralogical characteristics of poorly crystallized precipitates formed by oxidation of Fe^{2+} in acid sulfate waters. In: Alpers, N., Blowes, D.W. (Eds.), Environmental Geochemistry of Sulfide Oxidation. American Chemical Society, Washington, pp. 190–200.

Nordstrom, D.K., 1977. Hydrogeochemical and Microbiological Factors Affecting the Heavy Metal Geochemistry of an Acid Mine Drainage System. Ph.D. thesis, Stanford University, USA.

Paktunc, D., Dutrizac, E., 2003. Characterization of arsenate-for-sulfate substitution in synthetic jarosite using X-ray diffraction and X-ray absorption spectroscopy. Can. Mineral. 41, 905–919.

Paktunc, D., Foster, A., Heald, S., Laflamme, G., 2004. Speciation and characterization of arsenic in gold ores and cyanation tailings using X-ray absorption spectroscopy. Geochim. Cosmochim. Acta 68, 969–983.

Pelton, W.H., Ward, S.H., Hallof, P.G., Sill, W.R., Nelson, P.H., 1976. Mineral discrimination and removal of inductive coupling with multifrequency IP. Geophysics 43, 588–609.

Perry, R.S., Lynne, B.Y., Sephton, M.A., Kolb, V.A., Perry, C.C., Staley, J.T., 2006. Baking black opal in the desert sun; the importance of silica in desert varnish. Geology Boulder 34, 537–540.

Rammlmair, D., 1996. The role of gels in self organisation of slagheaps from the arsenic production site Muldenhütten, Freiberg, Saxony, FRG. In: Proceedings of Fifth International Congress Applied Mineralogy in the Minerals Industry, Warsaw 1996, Subdan-Druk, Warszawa, Poland, pp. 378–382.

Rammlmair, D., 2002. Hard pan formation on mining residuals. In: Merkel, B., Planer-Friedrich, B., Wolkersdorfer, C. (Eds), Uranium in the Aquatic Environment. In: Proceedings of International Conference Uranium Mining and Hydrogeology III and International Mine Water Assocation Symposium. TU Bergakademie Freiberg, Germany, pp. 173–182.

Rammlmair, D., Graupner, T., Klosa, D., Melcher, F., Lodziak, J., 2005. Alteration and precipitation pattern within a slagheap from an iron production site. Eur. J. Min. 17, 106, Beiheft 1.

Robins, R.G., 1987. Arsenic hydrometallurgy. In: Reddy, R.G., Hendrix, J.L., Queneau, P.B. (Eds.), Arsenic Metallurgy Fundamentals and Applications. TMS, pp. 215–247.

Rousel, C., Bril, H., Fernandez, A., 1999. Evolution of sulfide-rich mine tailings and immobilization of As and Fe. C.R. Acad. Sci. Paris Earth Planet Sci. 329, 787–794.

Sand, W., Gehrke, T., Jozsa, P.-G., Schippers, A., 2001. (Bio)chemistry of bacterial leaching – direct vs. indirect bioleaching. Hydrometallurgy 59, 159–175.

Schippers, A., 2004. Biogeochemistry of metal sulphide oxidation in mining environments, sediments, and soils. In: Amend, J.P., Edwards, K.J., Lyons, T.W. (Eds.), Sulfur Biogeochemistry – Past and Present. Special Paper 379. Geological Society of America, pp. 49–62.

Schippers, A., Bosecker, K., 2005. Bioleaching: Analysis of microbial communities dissolving metal sulfides. In: Barredo, J.-L. (Ed.), Methods in Biotechnology. Microbial Processes and Products, vol. 18. Humana Press Inc., Totowa, NJ, USA, pp. 405–412.

Schultze-Lam, S., Fortin, D., Davis, B.S., Beveridge, T.J., 1996. Mineralization on bacterial surfaces. Chem. Geol. 132, 171–181.

Scott, K.M., 1987. Solid-solution in, and classification of, gossan-derived members of the alunite–jarosite family, Northwest Queensland, Australia. Am. Mineral. 72, 178–187.

Southam, G., Beveridge, T.J., 1992. Enumeration of *Thiobacilli* within pH-neutral and acidic mine tailings and their role in the development of secondary mineral soil. Appl. Environ. Microbiol. 58, 1904–1912.

Starkey, R.L., 1925. Concerning the physiology of *Thiobacillus thiooxidans*, an autotrophic bacterium oxidizing sulfur under acid conditions. J. Bacteriol. 10, 135–162.

Steefel, C.I., van Cappellen, P., 1990. A new kinetic approach to modelling water–rock interaction: the role of nucleation, precursors, and Ostwald ripening. Geochim. Cosmochim. Acta 54, 2657–2677.

Tassé, N., Germain, D., Dufour, C., Tremblay, R., 1997. Hardpan formation in the Canadian Malartic mine tailings: implications for the reclamation of the abandoned impoundment. In: Fourth International Conference on Acid Rock Drainage. CANMET, Natural Resource Canada, Ottawa, vol. 4, pp. 1797–1812.

Tichomirowa, M., 2001. The gneiss of the ore mountains – high-grade metamorphic equivalents of Neoproterozoic–Early Palaeoizoic graywacke and granitoids of the Cadomids. Unpublished Habilitation thesis, Freiberg, Germany (in German).

Tichomirowa, M., Pelkner, S., Junghans, M., Haubrich, F., 2002. Sulfide oxidation at the polymetallic sulfide deposit Freiberg (Germany) and consequences for heavy metal mobilization. In: Schulz, H.D., Hadeler, A. (Eds.), Geochemical Processes in Soil and Groundwater. Measurement – Modelling – Upscaling, GeoProc 2002. Wiley–VCH, pp. 356–379.

Tuovinen, O.H., Bhatti, T.M., Bigham, J.M., Hallberg, K.B., Garcia Jr., O., Lindström, E.B., 1994. Oxidative dissolution of arsenopyrite by mesophilic and moderately thermophilic acidophiles. Appl. Environ. Microbiol. 60, 3268–3274.

Vlasceanu, L., Sarbu, S., Engel, A.S., Kinkle, B.K., 2000. Acidic cave-wall biofilms located in the Farasassi Gorge, Italy. Geomicrobiol. J. 17, 125–139.

Wan, J., Tokunaga, T.K., Saiz, E., Larsen, J.T., Zheng, Z., Couture, R.A., 2004. Colloid formation at waste plume fronts. Environ. Sci. Technol. 38, 6066–6073.

Waychunas, G.A., Davis, J.A., Fuller, C.C., 1995. Geometry of sorbed arsenate on ferrihydrite and crystalline FeOOH: Re-evaluation of EXAFS results and topological factors in predicting sorbate geometry, and evidence for monodentate complexes. Geochim. Cosmochim. Acta 59, 3655–3661.

Yunmei, Y., Yongxuan, Z., Williams-Jones, A.E., Zhenmin, G., Dexian, L., 2004. A kinetic study of the oxidation of arsenopyrite in acidic solutions: implications for the environment. Appl. Geochem. 19, 435–444.

Zeien, H., 1995. Chemische Extraktionen zur Bestimmung der Bindungsformen von Schwermetallen in Böden. Bonner Bodenkundl. Abh., 17.